Ocean Engineering 342 (2025) 122825

Contents lists available at ScienceDirect

Ocean Engineering

journal homepage: www.elsevier.com/locate/oceaneng

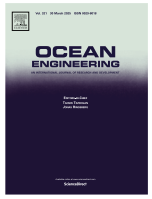

Research paper

# A model for motion-induced comfort assessment during the concept design phase of small cruise ships

F. Mauro [a,*], S. Utzeri [a], J. Prpić-Oršić [b], L. Braidotti [a], S. Bertagna [a], V. Bucci [a]

[a] Department of Engineering and Architecture, University of Trieste, Via Valerio 10, Trieste, 34100, Italy
[b] Faculty of Engineering, University of Rijeka, Vukovarska 58, Rijeka, 58000, Croatia

ARTICLE INFO

*Keywords:*
Cruise ships
Comfort
Regression analysis
Concept design
Vertical motions

ABSTRACT

One key aspect of cruise ship design is satisfaction with the onboard motion-induced comfort standards. Such standards imply evaluating motion-related indices, such as the motion sickness index (MSI), in several locations along the vessel. The assessment requires dedicated seakeeping calculations to predict vertical accelerations in the selected locations for comfort analysis. The requirements of the seakeeping calculations force designers to tackle this issue in a relatively advanced design stage, with hull form and the general layout already fixed. However, the comfort issue should be addressed already in the concept design phase, proposing an effective design strategy oriented to comfort satisfaction. To this end, the present article proposes a methodology for the comfort assessment of cruise ships in the concept design phase. Starting from a database of 25 vessels where seakeeping calculations are available for head seas at several speeds, dedicated regression formulae have been developed for the vertical motion transfer functions (TRFs). The Fourier model employed to regress the real and imaginary parts of the TRFs fits well with the initial database. Furthermore, the model has been tested on an external ship and compared with the standard procedure for MSI evaluation in a sea area of interest, showing good agreement with the obtained results.

## 1. Introduction

Cruise ships are complex objects to design, requiring the satisfaction of multiple goals in the design process (Andrews, 1998). As such, a designer should check the required standards from the early stages of the design, i.e. the concept phase (Caprace and Rigo, 2011). To this end, it is necessary to identify the most relevant attributes to assess and develop suitable mathematical models capable of predicting the main quantities with sufficient reliability (Papanikolaou, 2014, 2019). Traditionally, these metamodels concern the propulsive performances of the vessel (Trincas, 1989; Žanić et al., 1997; Mauro et al., 2025), intact stability (Mauro et al., 2019b), structural strengths (Žanić, 2013; Žanić and Čudina, 2009; Andric et al., 2021; Pintilie et al., 2025) and operational costs expressed as a function of main dimensions and geometrical parameters (Grubišić et al., 1997; Mauro et al., 2019a; Wang et al., 2025; Park et al., 2025). Other attributes are analysed only in a more advanced design stage, with the main particulars of the vessel fixed and the ship's general arrangement available (Papanikolaou, 2014). In this advanced stage, a designer assesses relevant topics like damage stability (Vassalos et al., 2022), motion assessment (Nabergoj, 2011; Seo et al., 2017) and onboard plant design (Barone et al., 2021). However, the availability of a database of previous designs, where all these additional issues have already been assessed, allows for building metamodels that can be employed in a concept phase, thus providing an instrument that helps designers make a proper design choice in the concept stage (Trincas, 2001; Bucci et al., 2021).

The availability of reliable data for the development of metamodels is crucial. Therefore, the assessment of desired attributes must employ high-fidelity, validated first-principle tools to ensure the reliability of the surrogate models (Mauro et al., 2023). Although recent developments in ship design promote the direct employment of first-principle tools for concurrent attribute determination (Papanikolaou et al., 2022; Zaraphonitis et al., 2020; Mauro and Vassalos, 2024a), it is the opinion that, for a concept phase, the use of surrogate models is still a valuable solution for its fast response and capability of studying multiple designs options (Jiang et al., 2020). Then, an accurate development of reliable models for the ship's attributes is necessary. According to this strategy, several high-fidelity surrogate models are available for different kinds of ships, targeting different attributes. However, the models address mainly issues related to resistance and propulsion in calm water (Holtrop, 1984; Radojčić et al., 2017) or added resistance in waves (Liu and Papanikolaou, 2016, 2020). Concerning ship motions,

* Corresponding author.
*E-mail addresses:* fmauro@units.it (F. Mauro), samuele.utzeri@phd.units.it (S. Utzeri).

https://doi.org/10.1016/j.oceaneng.2025.122825
Received 18 May 2025; Received in revised form 14 August 2025; Accepted 10 September 2025
Available online 23 September 2025

**Table 1**
Comfort-related ship motion criteria for pleasure vessels.

| Criterion Name | Quantity | Criteria fulfillment |
|---|---|---|
| ISO-22834 Yachts | $EGA$ and $MSI$ | $RMS(EGA) < 2$ deg<br>$MSI < 10\,\%$ |
| ISO 2631-1 | $MSI$ | $MSI < 10\,\%$ |
| MARIN comfort rating for passenger ships | $MIR$ | $MIR < 10$ (for passengers)<br>$MIR < 20$ (for crew members) |
| Nordforsk | Vertical acceleration | $RMS < 0.02g$ |
| | Lateral acceleration | $RMS < 0.03g$ |
| | Roll | $RMS < 2$ deg |
| Vibration Dose Value | $VDV$ | $VDV < 1$ |

the only models available in the literature refer to fishing boats (Sayli et al., 2007), half-displacement ships (Kapsenberg et al., 2015) or offshore applications (Mauro and Dell'Acqua, 2018). No specific models are available for cruise ships.

The present study on cruise ships develops a surrogate model for comfort performance prediction, filling a gap found in the literature. Specific models have been created for the transfer functions of heave and pitch motions for head seas at different speeds, starting from an initial database of 25 cruise vessels, with available hydrodynamic calculations for vertical motions. The developed model considers the transfer functions in the complex form, providing regressions for the real and imaginary parts in the form of a Fourier polynomial. Thanks to this strategy, estimating comfort-related indices like the Motion Sickness Index (MSI) along different locations of the ship is possible.

The work provides all the assumptions made for the model development and the descriptions of methods and tools employed for its realisation by following the upcoming structure:

- Section 2: description of comfort indices for passenger ships and selection of the most suitable index for this development.
- Section 3: presentation of the database of cruise ships and transfer functions.
- Section 4: explanation of the regression methodology employed for the transfer functions and presentation of the quality of fit of the obtained models.
- Section 5: application of the surrogate models to the case of a passenger ship external to the database. Process verification for comfort assessment compared to standard analyses.
- Section 6: identification of strengths and weaknesses of the process, identifying possible future studies for improvements.

The methodology developed in this study is the first attempt to estimate the comfort characteristics of cruise ships in the concept design stage. This study shows a good agreement with conventional comfort estimation methods employed in advanced stages of design, as highlighted by the presented test case. All the details and justifications of the present methodology are described in the following sections.

## 2. Comfort onboard cruise ships

Estimating comfort onboard is a key parameter for cruise ship design. However, determining unified standards for comfort is difficult as the definition of comfort implies subjective people's feelings. Moreover, many factors influence comfort perception, such as time to exposure, the intensity of the phenomenon, gender, age, previous experience and mental state of the subject. As an example, the following are the main influencing factors for a pleasure craft:

- Onboard amenities, food and drinks.
- Smell.
- Motions and postural stability.
- Noise and vibrations.
- Other factors (e.g. weather, temperature, humidity).

The paper focuses on wave-induced motions, discarding the other comfort components from the analysis. Therefore, motion-related criteria pertinent to comfort onboard passenger ships must be identified. The literature provides general criteria applicable to passenger vessels (Grin et al., 2013; NORDFORSK, 1987; ISO, 1997) or other pleasure craft like large motor yachts (ISO, 2022). Table 1 provides an overview of such criteria, having different indices and associated thresholds.

The first criterion concerns large yachts and is implemented in the ISO 22,834 standards (ISO, 2022; Mauro et al., 2021). The criterion considers the Effective Gravity Angle ($EGA$) and the Motion Sickness Index ($MSI$). The standard requires the evaluation of both indices for two speeds (0 and 12 knots), one heading (135 deg), five locations onboard and a predetermined set of sea states. $MSI$ is also used as comfort metrics by the ISO 2631-1 standards (ISO, 1997). Another option, more oriented to cruise ships, is given by the MARIN comfort rating (Grin et al., 2013). The criterion employs the Motion Illness Rating ($MIR$) to assess comfort. However, the index formulation requires knowledge of parameters and coefficients that are not available in the open literature or not easy to estimate in a concept design phase. NORDFORSK (1987) gives one of the most general criteria applicable to passenger ships. It considers the Root Means Square ($RMS$) values of the vertical and lateral acceleration of the vessel and the roll angle. The last option is the Vibration Dose Value ($VDV$) (Griffin and Whitham, 1980). The index is a function of the vertical accelerations of the ship, and its determination requires a weighted integration of the accelerations in a given period.

All these indices can be employed to classify comfort onboard passenger ships and cruise ships in particular. However, for the study's purposes, a selection should be made to target the most suitable options for concept design.

### 2.1. Selected criteria for comfort analysis

Some preliminary considerations are needed to identify the most suitable indices for the cruise ship comfort assessment in the concept design phase. The first consideration concerns the availability of data. In this sense, all the quantities needed for an index estimation should be available in the concept design stage. This requires surrogate models employed in the design process to be capable of estimating with sufficient accuracy all the needed parameters. Ship motions are sensitive to inertia and the position of the centre of gravity; this is true for vertical motions but is even more critical for lateral motions like roll. In the early design stage, inertia and centre of gravity estimation are subject to many uncertainties; therefore, considering attributes strongly influenced by such variables is unreliable.

Another consideration is the reliability of the motion surrogate models. The best option for ship motions is to deal with initial experimental data, which means having a database of ships composed of a full set of experimental data. This is a utopistic assumption as, in reality, it is most probable to deal with databases filled by hydrodynamic calculations. As such, the data reliability reflects the numerical method employed to solve the ship motion problem. Also, in this case, vertical motion reliability is less influenced by numerical resolution than lateral ones.

Therefore, between the several options described above, the most suitable indices for motion-induced comfort assessment in the concept design stage should be related to vertical motions. Then, the criteria

to apply could be the ones proposed by ISO 22,834 and Nordfosk. ISO criterion is developed for yachts but the thresholds for indices derive from passenger vessels. However, ISO 22,834 considers EGA and MSI. The formulation of $EGA$ is as follows:

$$EGA = \arctan \frac{\ddot{\eta}}{\ddot{\zeta} + g} \tag{1}$$

where $\ddot{\eta}$ is the lateral acceleration and $\ddot{\zeta}$ the vertical acceleration in a given location. Then, lateral accelerations influence $EGA$, which, consequently, is not a suitable indicator for comfort assessment in the concept design stage. Therefore, the criteria selected for the concept design stage analysis of comfort for cruise ships are:

- Vertical acceleration below 0.02 g according to Nordfosk indications.
- $MSI$ below 10 % after 2 h of exposure according to ISO 22834.

The estimation of $MSI$ considers the following formulation, as applied in the ISO 22,834 criterion:

$$MSI = 100\Phi(Z_\zeta)\Phi(Z_t') \tag{2}$$

with:

$$Z_\zeta = 2.128 \log \ddot{\zeta}/g - 9.277\hat{\omega_\zeta} - 5.809\hat{\omega_\zeta}^2 - 1.851 \tag{3}$$

$$Z_t' = 1.134 Z_\zeta + 1.989 \log T_e - 2.904 \tag{4}$$

$$\Phi(Z) = \frac{1}{\sqrt{2\pi}} \int_{-\infty}^{Z} \exp\left(-x^2/2\right) \mathrm{d}x \tag{5}$$

where $T_e$ is the exposure time in minutes and $\omega_\zeta$ is the frequency in Hertz of the absolute vertical acceleration $\ddot{\zeta}$ spectrum's peak. This is a simplified version of $MSI$, which includes only effects due to vertical accelerations. This preliminary study considers only the case of head seas (thus neglecting effects associated with lateral motions), where the reliability of seakeeping solvers is sufficiently high, for two different speeds: the design speed and the transfer speed. Besides these two assumptions concerning speed and heading, particular attention should be paid to the locations for the comfort criteria evaluation and the environmental conditions for the motion calculations.

### 2.2. Locations and environmental conditions

When evaluating comfort onboard, it is essential to identify the specific locations for motion calculations and the relevant environmental conditions to consider (Begovic et al., 2023).

Concerning locations, there are no general guidelines for selecting the focus points for a comfort analysis. However, indications could be given by standards developed for other leisure crafts. According to the ISO 22,834 standard for yachts, comfort is assessed at five distinct locations representing the leisure areas for passengers and the working areas for crew members. Comfort assessment on cruise ships could follow the same strategy. The present work does not aim to present a standard to follow, as any design has its peculiarities, and a designer should be allowed to choose the most appropriate locations of interest. However, for this study, the following locations have been selected as representative:

- Swimming pool deck.
- Principal attraction (e.g. theatre, restaurants, etc.) deck.
- Main suites.
- Wheel house.

As the locations are not fixed in all designs, the surrogate model needed to predict $MSI$ and vertical acceleration should be capable of considering any point along the vessel. For such a reason, as will be further discussed in the model development section, it is not sufficient to consider only the motion transfer function amplitude of the centre of gravity. The model should also include the phase to evaluate motion in general points along the ship.

The second issue involves selecting the environmental conditions for comfort analysis, i.e. determining the couples of significant wave heights $H_s$ and zero-crossing periods $T_z$ relevant to the vessel operative profile. This implies using Wave Scatter Diagrams available in the literature, direct measurements or data derived by hindcast-forecast predictions. However, the operative profile of a cruise ship is changing design by design, and sometimes, a ship could operate in different reference sea areas during the life cycle. For this purpose, it is proposed to use a weighted equivalent scatter diagram composed of a weighted average of the $H_s$ and $T_z$ occurrences in the areas of interest of the operations. This study considers the most common sea areas of operation for cruise ships as operative profiles, namely the Caribbean Sea and the Western and Eastern Mediterranean (corresponding to Area 47, 26 and 27 of the Global Wave Statistics (Hogben et al., 1986)). At this stage, the weights between the areas are equal. Then, a JONSWAP spectrum (Hasselmann and Olbers, 1973) with variable elongation parameter $\gamma$ (Mauro and Vassalos, 2024b) is employed for each couple of $H_s$ and $T_z$ to evaluate $MSI$ and vertical acceleration $\ddot{\zeta}$. The employment of this kind of spectrum allows for generating a generic sea state according to the different wave parameters (DNV, 2014). The modelling allows for generating sea states representative of seas in formation (case with $\gamma > 1$) and cases of full developed seas ($\gamma = 1$). More specifically, the cases with $\gamma = 1$ corresponds to the employment of a Bretschneider spectrum.

With locations and the environmental conditions defined, the comfort rating of the vessel can be calculated at each speed $V$ of interest:

$$CR_V = \sum_{i=1}^{N_{T_z}} \sum_{j=1}^{N_{H_s}} \sum_{k=1}^{N_L} p_{w_{ij}} p_{L_k} I_{CR_{ijk}} \tag{6}$$

where $p_w$ is the joint distribution of $H_s$ and $T_z$, $p_L$ is the weight given to each location, $N_L$ is the number of locations, $N_{T_z}$ the number of wave periods and $N_{H_s}$ the number of wave heights. Function $I_{CR}$ is defined as follows:

$$I_{CR_{ijk}} = \begin{cases} 1 & \text{if } MSI_{ijk} < 10\,\% \wedge \ddot{\zeta}_{ijk} < 0.02g \\ 0 & \text{otherwise} \end{cases} \tag{7}$$

While it is desired to evaluate only the $CR$ in the specific locations at each speed, then the formula is simplified and becomes:

$$CR_{VL} = \sum_{i=1}^{N_{T_z}} \sum_{j=1}^{N_{H_s}} p_{w_{ij}} I_{CR_{ij}} \tag{8}$$

The comfort rating $CR$ can be considered at each speed or, as an alternative, could be weighted between the speeds obtaining a single global value.

### 2.3. Framework for concept design

The assumptions and considerations explained in the previous section are fundamental for defining a framework for the motion-induced comfort of passenger ships in the concept design phase. The framework should be applicable in the attribute selection process of the concept design phase, thus employing the same independent variables used for the concurrent generation of different design options. Therefore, for each project, the framework follows the subsequent process:

- *Identification of locations*: establishing the selected locations for the comfort analysis according to the ship's main dimensions.
- *Operational profile*: selection of the operational areas of the vessel for determining relevant $H_s - T_z$ combinations.
- *Transfer functions for barycentric motions*: calculation of vertical motions transfer functions in a given frequency range with a surrogate model.
- *Local transfer functions*: evaluation of transfer functions for the different locations.
- *Comfort analysis*: evaluation of $MSI$ and $\ddot{\zeta}$ for all locations, speeds and environmental conditions.
- *Comfort rating*: evaluation of the $CR$ for the ship.

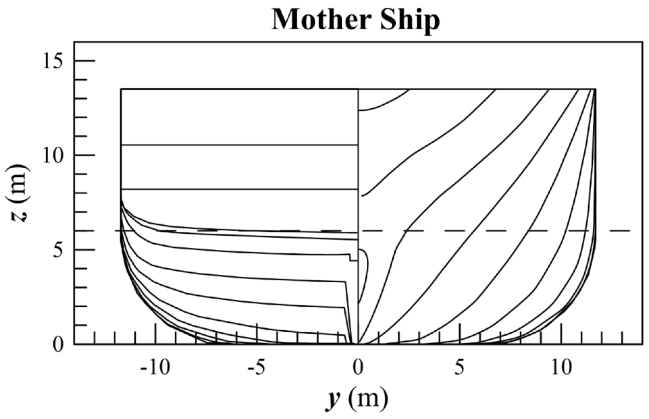


**Fig. 1.** Transversal sections of the mother ship.

**Table 2**
General particulars of the mother ship.

| | Symbol | Value | Unit |
|---|---|---|---|
| Length between perpendiculars | $L_{PP}$ | 170.78 | m |
| Waterline length | $L_{WL}$ | 174.21 | m |
| Breadth | $B$ | 24.75 | m |
| Draught | $T$ | 6.00 | m |
| Volume | $\nabla$ | 17374.83 | $m^3$ |
| Wetted surface | $S$ | 5152.884 | $m^2$ |
| Longitudinal centre of buoyancy | $x_B$ | 88.21 | m |
| Vertical centre of buoyancy | $z_B$ | 3.36 | m |
| Block coefficient | $C_B$ | 0.685 | – |
| Prismatic coefficient | $C_P$ | 0.725 | – |
| Midship coefficient | $C_x$ | 0.945 | – |
| Length/Breadth ratio | $L/B$ | 6.900 | – |
| Breath/Draught ratio | $B/T$ | 4.125 | – |

The process outlined above allows for determining the motion-induced comfort rating of each concurrent project created in a concept design stage selection procedure.

As highlighted by the process, evaluating comfort requires the availability of a surrogate model for the vertical motion transfer functions. This model should be tailored to the design space employed for the concept design selection procedure, thus requiring original data coming from a database covering the target design space. The following sections discuss the formation of the database and the methodologies employed to develop the surrogate model.

## 3. Ships database

In the open literature, there is no open database containing the hull forms necessary to perform direct hydrodynamic calculations to estimate the motion transfer functions of a cruise vessel. Therefore, it is necessary to generate a suitable database to be capable of performing such calculations. To this end, techniques like the Design of Experiments (DoE) (Box et al., 2005) could help in generating a design space, starting from an initial hull form, selecting an opportune number of variations for a set of given geometrical parameters.

In the present study, the ship presented in Fig. 1 is selected as the reference point for the initial database development. The main particulars of the vessel are reported in Table 2. Starting from this mother ship, a design space of 25 hulls has been developed. The coming sections describe the DoE technique and the geometry transformations employed for the hull database development, together with the assumptions, methods and results of the preliminary hydrodynamic calculations performed to obtain the TRFs.

### 3.1. Design of experiments

The database employed in this study is taken from a previous study related to the development of initial stability models for cruise ships (DiGregorio, 2020). All the hulls of the database have the same Draught $T$ of 6.0 metres. $T$ is considered constant as it is the dimension having less statistical variations for vessels having sizes comparable with the mother ship. Therefore, the design strategy employed for the database was considering variations of five main hull parameters:

- Length/Breadth ratio $L/B$
- Breadth/Draught ratio $B/T$
- Depth/Draught ratio $D/T$
- Midship coefficient $C_x$
- Prismatic coefficient $C_P$

**Table 3**
General particulars of the 25 hull forms.

| | $L/B$ [-] | $B/T$ [-] | $C_x$ [-] | $C_P$ [-] | $L_{PP}$ [m] | $B$ [m] | $T$ [m] | $\nabla$ [$m^3$] | $x_B$ [m] | $z_G$ [m] |
|---|---|---|---|---|---|---|---|---|---|---|
| Hull 01 | 6.900 | 4.125 | 0.945 | 0.725 | 170.78 | 24.75 | 6.00 | 17374.83 | 88.21 | 11.16 |
| Hull 02 | 6.600 | 3.900 | 0.900 | 0.700 | 154.44 | 23.40 | 6.00 | 13660.53 | 79.64 | 10.35 |
| Hull 03 | 6.600 | 3.900 | 0.900 | 0.750 | 154.44 | 23.40 | 6.00 | 14636.28 | 79.62 | 10.03 |
| Hull 04 | 6.600 | 3.900 | 0.990 | 0.700 | 154.44 | 23.40 | 6.00 | 15026.58 | 79.22 | 9.97 |
| Hull 05 | 6.600 | 3.900 | 0.990 | 0.750 | 154.44 | 23.40 | 6.00 | 16099.91 | 79.18 | 9.91 |
| Hull 06 | 6.600 | 4.350 | 0.900 | 0.700 | 172.26 | 26.10 | 6.00 | 16994.83 | 88.90 | 10.14 |
| Hull 07 | 6.600 | 4.350 | 0.990 | 0.700 | 172.26 | 26.10 | 6.00 | 18694.31 | 88.53 | 10.02 |
| Hull 08 | 6.600 | 4.350 | 0.900 | 0.750 | 172.26 | 26.10 | 6.00 | 18208.74 | 88.87 | 10.09 |
| Hull 09 | 6.600 | 4.350 | 0.990 | 0.750 | 172.26 | 26.10 | 6.00 | 20029.62 | 88.38 | 9.91 |
| Hull 10 | 7.200 | 3.900 | 0.900 | 0.700 | 168.48 | 23.40 | 6.00 | 14902.39 | 86.91 | 10.19 |
| Hull 11 | 7.200 | 3.900 | 0.900 | 0.750 | 168.48 | 23.40 | 6.00 | 15966.85 | 86.88 | 10.02 |
| Hull 12 | 7.200 | 3.900 | 0.990 | 0.700 | 168.48 | 23.40 | 6.00 | 16392.63 | 86.56 | 10.11 |
| Hull 13 | 7.200 | 3.900 | 0.990 | 0.750 | 168.48 | 23.40 | 6.00 | 17563.53 | 86.49 | 9.91 |
| Hull 14 | 7.200 | 4.350 | 0.900 | 0.700 | 187.92 | 26.10 | 6.00 | 18539.81 | 97.01 | 10.35 |
| Hull 15 | 7.200 | 4.350 | 0.900 | 0.750 | 187.92 | 26.10 | 6.00 | 19864.08 | 96.97 | 10.03 |
| Hull 16 | 7.200 | 4.350 | 0.990 | 0.700 | 187.92 | 26.10 | 6.00 | 20393.79 | 96.61 | 9.95 |
| Hull 17 | 7.200 | 4.350 | 0.990 | 0.750 | 187.92 | 26.10 | 6.00 | 21850.49 | 96.53 | 9.90 |
| Hull 18 | 6.600 | 4.125 | 0.945 | 0.725 | 163.35 | 24.75 | 6.00 | 16619.40 | 84.35 | 11.06 |
| Hull 19 | 7.200 | 4.125 | 0.945 | 0.725 | 178.20 | 24.75 | 6.00 | 18130.26 | 92.05 | 11.14 |
| Hull 20 | 6.900 | 3.900 | 0.945 | 0.725 | 161.46 | 23.40 | 6.00 | 15531.09 | 83.36 | 11.23 |
| Hull 21 | 6.900 | 4.350 | 0.945 | 0.725 | 180.09 | 26.10 | 6.00 | 19321.96 | 93.05 | 11.05 |
| Hull 22 | 6.900 | 4.125 | 0.900 | 0.725 | 170.78 | 24.75 | 6.00 | 16547.46 | 88.27 | 11.22 |
| Hull 23 | 6.900 | 4.125 | 0.990 | 0.725 | 170.78 | 24.75 | 6.00 | 18202.20 | 87.69 | 10.98 |
| Hull 24 | 6.900 | 4.125 | 0.945 | 0.700 | 170.78 | 24.75 | 6.00 | 16775.70 | 87.94 | 11.04 |
| Hull 25 | 6.900 | 4.125 | 0.945 | 0.750 | 170.78 | 24.75 | 6.00 | 17973.96 | 87.92 | 11.01 |

The generation of the initial database has been performed starting from the mother ship reported in Table 2, considering the following limits for the five hull form parameters:

$$\begin{aligned} 6.600 < L/B < 7.200 \\ 3.900 < B/T < 4.350 \\ 0.364 < T/D < 0.444 \\ 0.900 < C_x < 0.990 \\ 0.700 < C_P < .750 \end{aligned} \tag{9}$$

To fill the design space, a Central Composite Design technique has been employed (Rodrigues and Iemma, 2014), more specifically an hybrid between a central faced model (CCF) and a full factorial design. Such an approach led to the definition of 43 hull forms, having different combinations of the above mentioned parameters.

The database has the ratio $T/D$ as one of the independent parameters; however, changes of such variable are not generating a different hull form as the form variation mainly involves the upper structure of the ship. Having the intention to perform hydrodynamic calculations, such changes are not captured by the calculation codes which considers only the submerged body of the ship. To this end, the present study considers a reduced version of the database, developing the database with a CCF model by changing $L/B$, $B/T$, $C_x$ and $C_P$ according to the limits reported in Eq. (9).

The resulting new CCF database is composed of 25 ships, having the main coefficients and dimensions as reported in Table 3. Fig. 2 shows the transversal sections of a subset of the 25 hull forms. From Table 3, it is possible to derive the range of changes in the dimensional values of the ship, in particular for the main dimensions and the volume $\nabla$. The

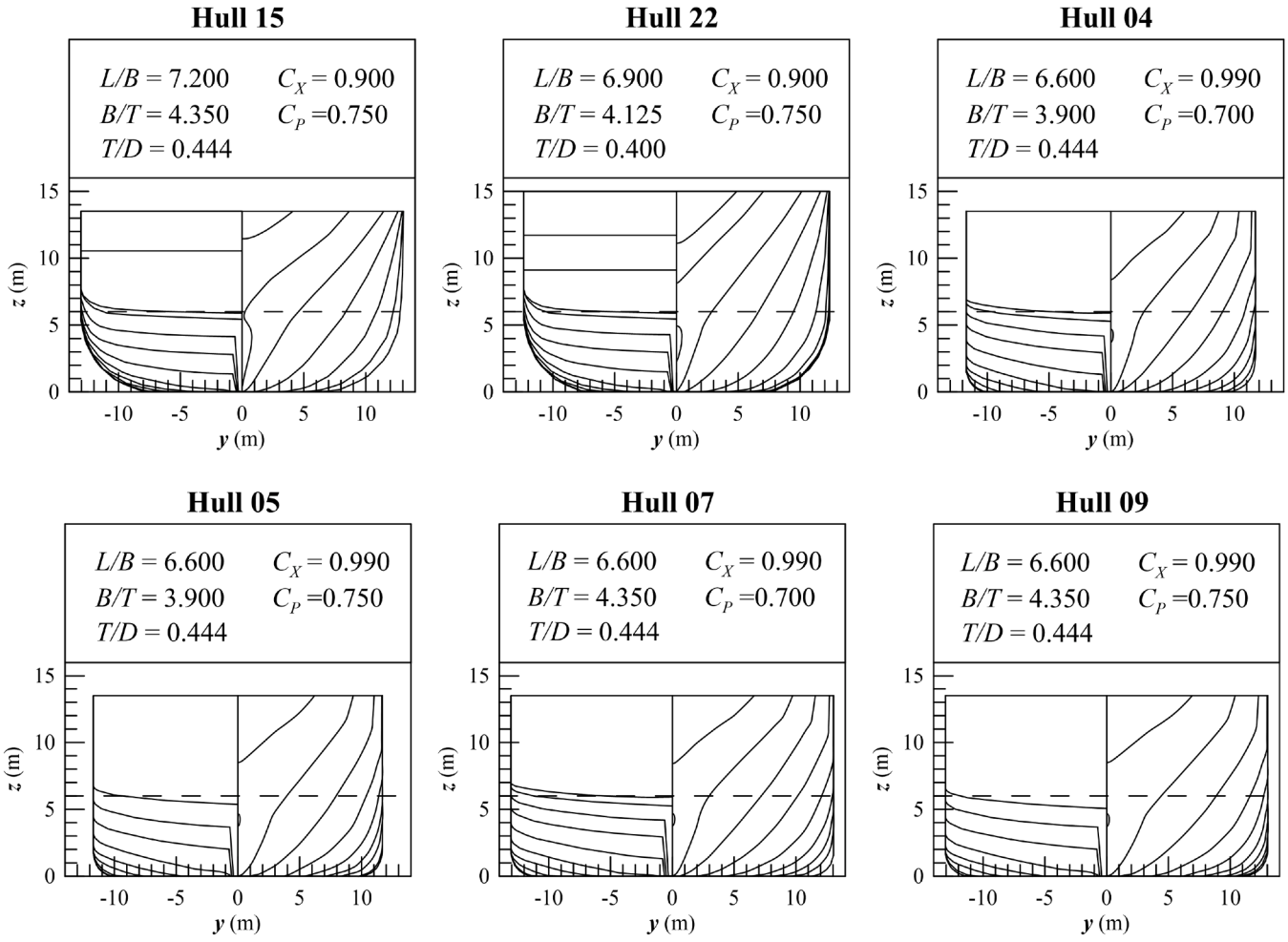


**Fig. 2.** Transversal sections of a subset of the ship database.

actual database covers a range from about 150.00 to 190.00 metres of $L_{PP}$, 23.00 to 26.00 metres of $B$ and $\nabla$ from 14,500.00 to 21,900.00 cubic metres. This is a reasonable range to cover the design of small cruise ships.

This composition of the database is the starting point for the determination of the vertical motions TRFs.

### 3.2. Transfer functions

The database of 25 ships, described in the previous section, is the starting point to develop a dataset of vertical motions transfer functions. To this end, it is relevant identify the calculation conditions and the methods employed for the hydrodynamic calculations.

Concerning the conditions, the encounter settings should be decided, means selecting the calculation headings and speeds. Aiming at determining a model for head seas, the encounter angle considered in the study is restricted to 180 degrees. For the selection of speeds, the operative profile of small cruise vessels has been considered. As such, the speed range between 10.0 and 20.0 knots has been identified, considering a discretisation in steps of 2.5 knots. This results in a total of 5 calculation speeds.

An important point to the hydrodynamic calculations is the definition of loading conditions of the ship. This includes the determination of the centre of gravity position and the inertia for all the 25 hulls. For the inertia, standard values have been employed in the calculations, setting the radii according to the following relations: $r_{xx} = 0.32B$, $r_{yy} = 0.25L_{PP}$ and $r_{zz} = 0.25L_{PP}$. Such values are reasonable for small cruise ships, as also highlighted from recent studies in the field (Grin et al., 2016; Grin, 2024). For the determination of the centre of gravity, different considerations have been done concerning the vertical $z_G$ and the longitudinal $x_G$ positions. The $x_G$ has been considered equal to the $x_B$, thus supposing that the vessel is sailing without trimming. For the vertical position $z_G$, a realistic loading condition has been derived for each ship (DiGregorio, 2020).

Dealing with vertical motions only, it has been decided to employ 2D strip theory (Salvesen et al., 1970) calculations to determine the TRFs. The Salvesen-Tuck-Faltinsen (STF) 2D strip method is a widely used semi-analytical technique for predicting a ship's seakeeping performance in waves. It divides the hull into a series of transverse 2D strips, solves the hydrodynamic problem for each cross-section using linear potential flow theory, and integrates the results along the ship's length to obtain motions and loads such as heave, pitch, and bending moments. Its main advantages are computational efficiency, relatively simple implementation, and good accuracy for slender, conventional hull forms in moderate sea states, making it ideal for preliminary design and optimization studies. It also allows quick parametric analyses and sensitivity checks without the heavy cost of 3D panel or CFD simulations. However, it is limited by its linear assumptions, which neglect nonlinear wave effects, viscous forces, and strong forward-speed effects in steep or breaking waves. The method also becomes less accurate for ships with bluff bows, shallow drafts, or extreme hull geometries. Despite these constraints, the STF strip method remains a standard early-stage seakeeping tool in naval architecture due to its speed, robustness, and reasonable accuracy. A state-of-the-art code has been employed to perform the hydrodynamic calculations on the above-mentioned encounter conditions, considering a frequency range between 0.3 and 1.0 rad/s. The

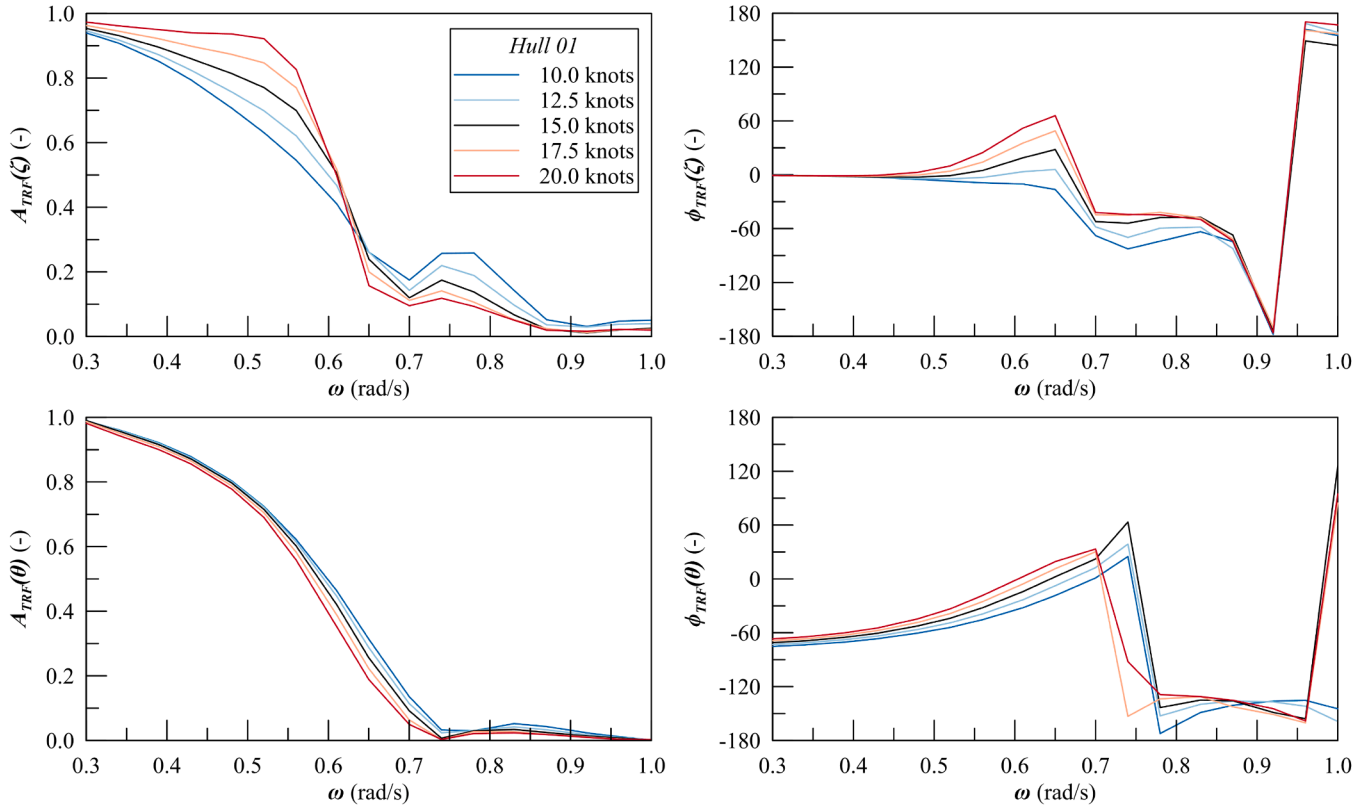


**Fig. 3.** Heave and pitch TRFs for ship hull 01 at different speeds.

calculated TRFs covers a wave length-to-ship length ratio range from approximately 0.35 to 4, encompassing the region where the largest motions typically occur, around a ratio of 1.0. In this case, the maximum pitch is observed at approximately 0.75 rad/s, corresponding to a wave length-to-ship length ratio of about 0.65, which lies within the range covered by the calculations. As a result, the amplitudes $A(\zeta)$ and $A(\theta)$ together with the phases $\phi(\zeta)$ and $\phi(\theta)$ have been evaluated for all the 25 hulls. As an example, Fig. 3 shows an example of the TRFs obtained on the database for the specific case of Hull 01.

The obtained TRFs are the starting dataset for the development of the regression model that will be discussed in the following section.

## 4. Regression model

Starting from the database of transfer functions ($TRFs$) described in Section 3, it is possible to evaluate the surrogate models as a function of the geometrical characteristics of the vessel. As mentioned in Section 2, the necessity of predicting the vertical accelerations in specific points of a vessel requires the availability not only of the amplitude of the transfer function but also of the phase.

Previous studies highlight that the direct regression of the phases does not provide a sufficiently accurate model for concept design phase purposes. Therefore, a different strategy needs to be applied for the predictions of motions. In this sense, an alternative method could be found in modelling the $TRFs$ in complex form, considering the following exponential formulation:

$$TRF(\omega) = A(\omega)e^{i\phi(\omega)} \tag{10}$$

where $A(\omega)$ is the $TRF$ amplitude and $\phi(\omega)$ is the $TRF$ phase as a function of the frequency $\omega$.

Here, it is proposed to perform the regression on the real and imaginary part of the $TRF$, having the following formulations:

$$Re_{TRF}(\omega) = A(\omega)\cos\phi(\omega) \tag{11}$$

$$Im_{TRF}(\omega) = A(\omega)\sin\phi(\omega) \tag{12}$$

According to the modelling provided by Eqs. (11) and (12), the transfer function is characterised by two oscillating continuous functions between $\omega_{\min}$ and $\omega_{\max}$ instead of a decaying amplitude and a discontinuous phase. Fig. 4 shows the real and imaginary part of the transfer function for heave and pitch at 10 knots for one of the vessels in the initial database. The figure highlights that the curves are continuous and smooth between the calculated frequency range, which is in contrast to the discontinuous behaviour of the phases shown in the previous section.

Dealing with two continuous functions facilitates the regression process, allowing to employ alternative regression techniques compared to what has been experimented with in the past. In the specific case, dealing with oscillating functions, a model based on Fourier analysis is proposed for both the real and imaginary parts. Thus, the real and the imaginary part of the $TRF$ could be regressed according to the following model:

$$\left.\begin{matrix} Re_{TRF}(\omega) \\ Im_{TRF}(\omega) \end{matrix}\right\} = a_0 + \sum_{i=1}^{N} a_i \cos\phi_i\omega + b_i \sin\phi_i\omega \tag{13}$$

where $a_i$ and $b_i$ are the $N$ Fourier series coefficients and $\phi$ is an auxiliary frequency vector.

The following subsections describe the steps necessary to implement the regression models according to the Fourier analysis.

### 4.1. Data preparation

As mentioned above, the real and imaginary parts of $TRF$ are oscillating functions in $\omega$, so it is possible to approximate them with a Fourier polynomial. However, some preliminary operations on the $TRFs$ are needed to optimise the performances of the Fourier analysis.

In the first place, the real and imaginary parts of $TRF$ do not start and end at the same value. Therefore, due to the Gibbs phenomenon,

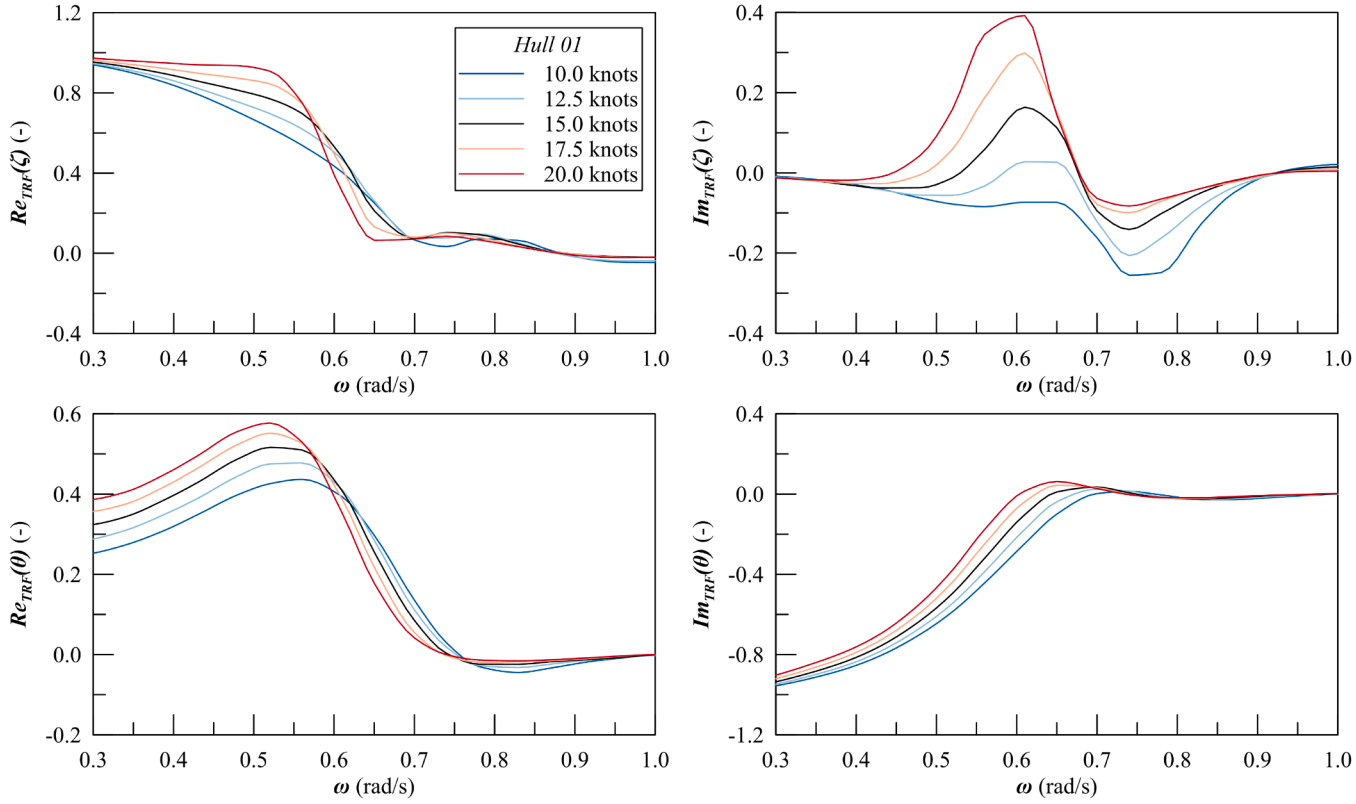


**Fig. 4.** Heave and pitch complex TRF for ship hull 01 at different speeds.

at the extremities of the $\omega$ domain, the approximating function passes through the midpoint of the discontinuity. To avoid that, the real and imaginary parts of the $TRFs$ have been extended for one period in $\omega$, reflecting the function around the $y$-axis. This transformation allows for obtaining a continuous function that starts and ends at the same $y$ value.

Another consideration concerns the frequency $\omega$ range. As highlighted in Section 3, the $TRFs$ database starts not from 0 but from 0.3 rad/s. To facilitate the regression process, an auxiliary frequency vector $\omega^*$ is considered, obtained as follows:

$$\omega^* = \omega - \min(\omega) \tag{14}$$

This transformation, together with the reflection introduced above, allows for obtaining an even function in $\omega^*$. The introduction of the auxiliary frequency $\omega^*$ is not related to the physics of the problem but allows for mathematical simplification in the Fourier polynomial employed for the regression analysis. Therefore, the associated Fourier polynomial has only terms in cosine and Eq. (13) can be rewritten as:

$$\left.\begin{matrix} Re_{TRF}(\omega^*) \\ Im_{TRF}(\omega^*) \end{matrix}\right\} = a_0 + \sum_{i=1}^{N} a_i \cos \phi_i \omega^* \tag{15}$$

An example of the obtained functions for the regression analysis is reported in Fig. 5 for the heave and in Fig. 6 for the pitch. The figures report the transformed complex $TRFs$ for four reference hulls, highlighting a variability of the curves, thus confirming the dependence of the functions on the main parameters of the hull. Having the dataset of real and imaginary parts as described above, it is possible to start with the Fourier analysis.

### 4.2. Fourier analysis

The first step of the regression analysis is to approximate the real and imaginary parts of $TRFs$ with a Fourier polynomial. According to the model described by Eq. (15), it is necessary to identify the number of harmonics $N$ of the polynomial.

$N$ is associated with the length of the sampling vector $\omega^*$. In this study, $\omega^*$ is sampled with a sampling frequency of 0.01 rad/s, resulting in a total of 140 intervals. Therefore, the maximum number of harmonics $N$, according to the Nyquist theorem, is defined as half of the intervals. Then, $N$ is equal to 70, with frequency intervals $\delta\phi$ of 4.488 rad/s. The Fourier analysis should be performed for each real and imaginary parts of heave and pitch, for 5 speeds and 43 hulls. This results in a total amount of 860 analyses and the determination of 60,200 Fourier coefficients $a_i$ plus 860 coefficients $a_0$. The total amount of coefficients is considerable; therefore, in the optics of developing useful surrogate models for the $TRFs$ it is convenient to analyse which ones are the significant harmonics for the real and imaginary parts reproduction.

Identification of significant harmonics entails determining which is the minimum amount of harmonics $N_H$ that allows for good reproduction of the analysed functions. To this end, use can be made of the determination index $R^2$, a quality of fit metrics defined in the following way:

$$R^2 = 1 - \frac{SSE}{SS_{tot}} \tag{16}$$

with:

$$SSE = \sum_{i=1}^{n} \left(y_i - f_i\right)^2 \tag{17}$$

$$SS_{tot} = \sum_{i=1}^{n} \left(y_i - \bar{y}\right) \tag{18}$$

$$\bar{y} = \frac{1}{n} \sum_{i=1}^{n} y_i \tag{19}$$

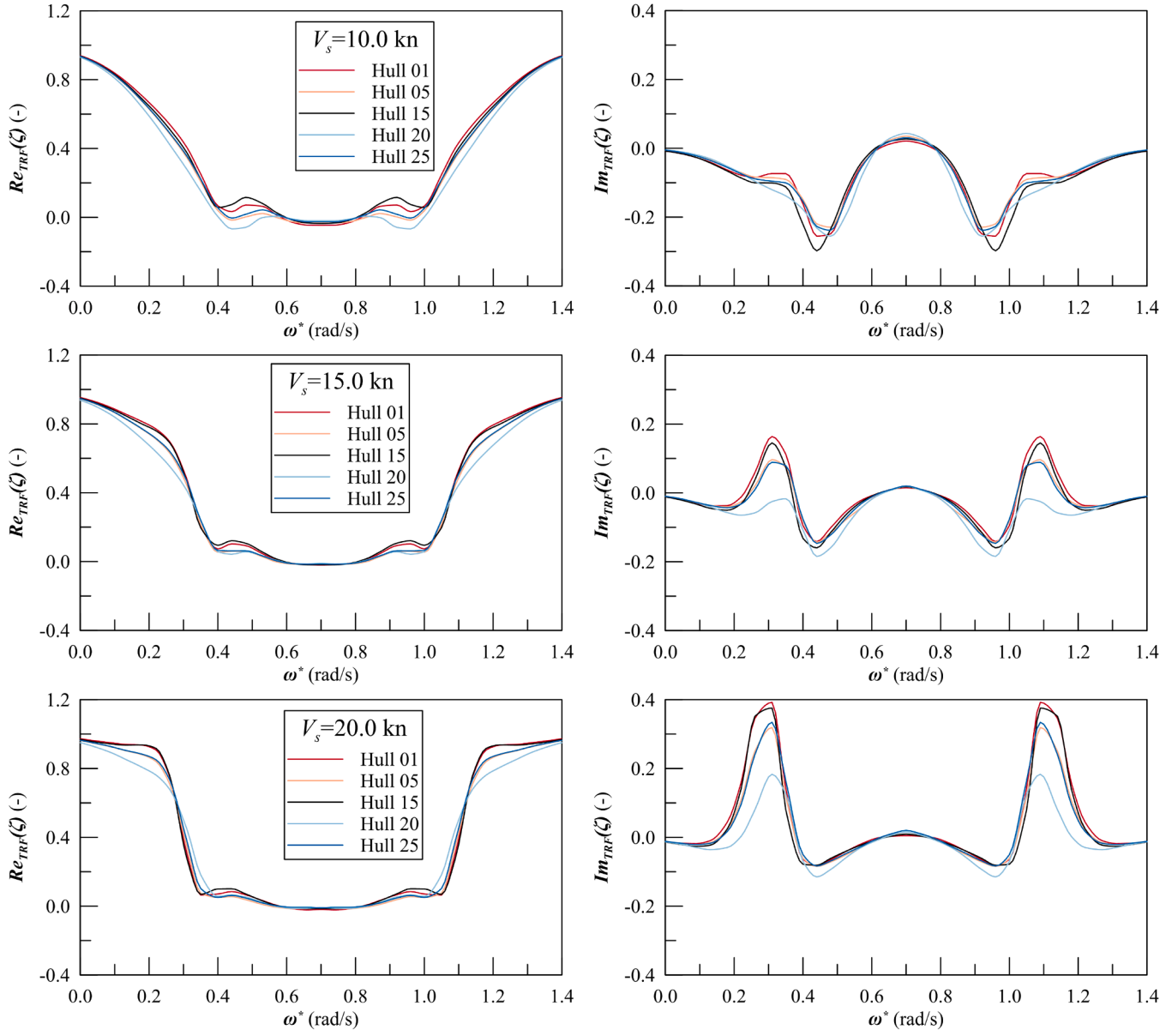


**Fig. 5.** Heave complex transfer functions at different speeds for Fourier analysis.

where $y_i$ are the $n$ points to fit and $f_i$ are the fitting values from the regression analysis. As the quality of fit assessment at this stage is involving only the comparison between two curves, the adoption of other quality of fit indicators is not needed, as it will give n added value to the indications provided by the $R^2$.

To identify the minimum number of harmonics needed for a reasonably acceptable fitting, an iterative process has been set up. Starting from considering only one harmonic, the number of regressor has been constantly increased by one until reaching $N$ harmonics. At each step, the $R^2$ is evaluated for the 43 vessels for real and imaginary parts of heave and pitch. Thanks to this approach, it is possible to identify the effect of adding a harmonic to the $R^2$. However, as the complex transfer functions are different per each ship, it is complicated to specifically identify a unique $N_H$ for all the ships. To this end, the following strategy has been employed:

- Evaluation of $R^2$ for all the ships.
- Identification of $\min\left(R_j^2\right)$ between the 43 ships.
- Check if $\min\left(R_j^2\right) \geq 0.998$.

The threshold of 0.998 has been selected because it has been observed that it grants that the regression function follows the original data without additional oscillations due to low-frequency harmonics.

By employing this strategy a unique number $N_H$ has been identified for each one of the regression groups. Table 4 reports the results of the analysis.

It can be observed that the Fourier polynomials for real and imaginary parts of the pitch motion require a relatively low number of harmonics to properly fit the $TRFs$. In fact they require an $N_H$ between 6 and 8, depending on the speed.

Different is the case of heave motion. Once the real part is considered, the harmonics number are still quite low, ranging from 8 to 9 according to the different speeds. On the other hand, the imaginary part is more complicated to fit, as a reasonable quality is reached only by considering 20 to 22 harmonics. This is mainly due to the shape of the imaginary function, which presents consistent oscillations at all the speeds as highlighted in Fig. 5. In any case, determining dedicated regression for the 22 harmonics needed to fit the function is not an obstacle to the application of such a model in the concept design stage.

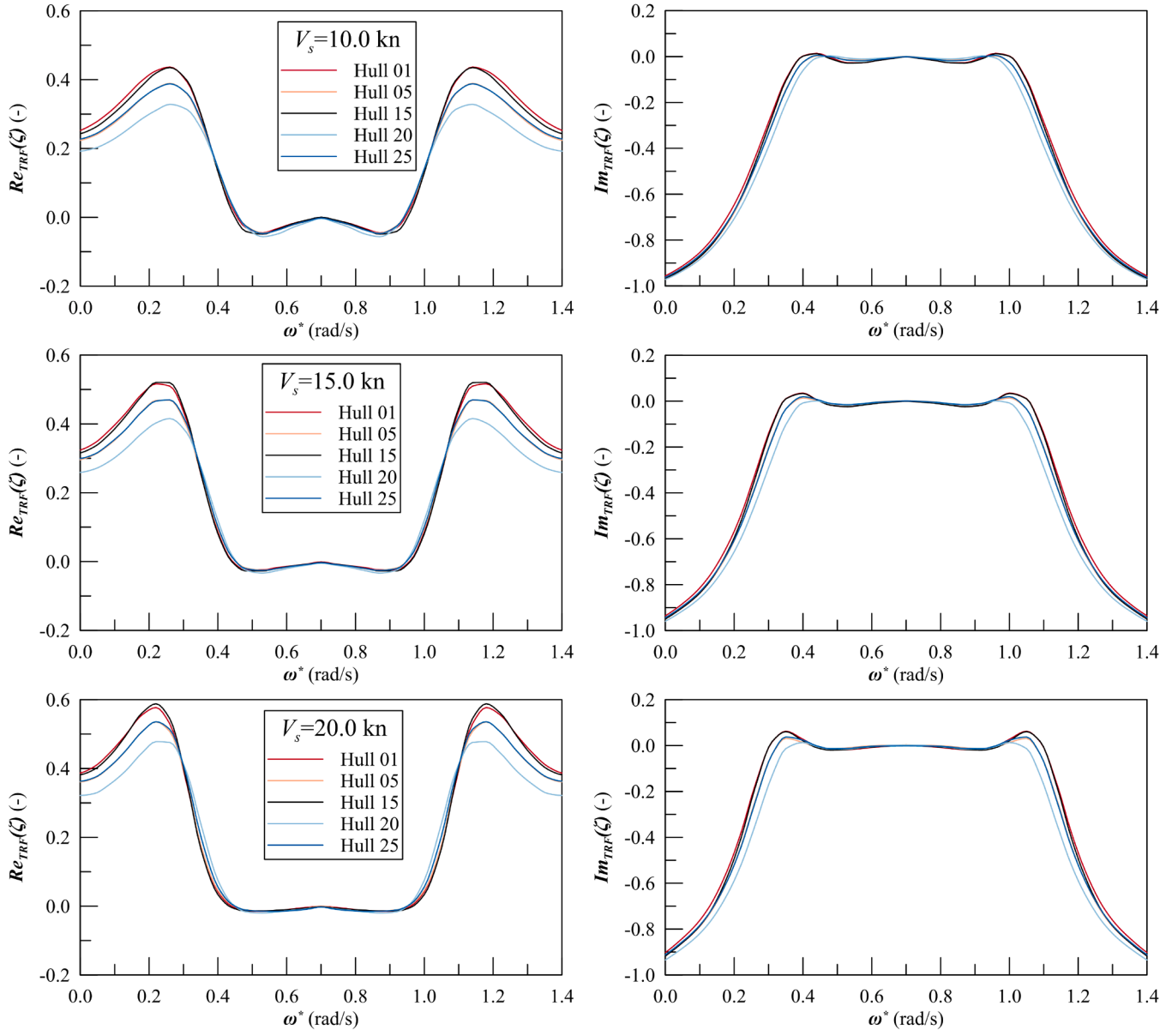


**Fig. 6.** Pitch complex transfer functions at different speeds for Fourier analysis.

Fig. 7 shows the trends of the calculated $\min\left(R^2\right)$ for each Fourier polynomial for heave and pitch real and imaginary part at the different speeds. The picture shows the asymptotic trends of the quality of fit, highlighting the fast convergence for pitch polynomials compared to the heave imaginary part. The obtained Fourier polynomials with $N_H$ harmonics are the starting point for developing the surrogate models of complex transfer functions.

### 4.3. Harmonics regressions and quality of fit

After having defined the number of harmonics $N_H$ necessary to adequately fit the real and imaginary part of the TRFs, it is necessary to find a correlation between the harmonics values and the hull form parameters of the ship database. Due to the relatively low size of the data and the nature of the CCF design employed to develop the database, a suitable method to derive the correlations is provided by Multiple Linear Regressions (MLR) (Weisberg, 2005).

MLR is a fundamental statistical technique used for modeling the relationship between a dependent variable and multiple independent variables. In statistical modeling, understanding the relationship between a dependent variable and one or more predictors is central to prediction. While simple linear regression addresses the case of a single predictor, most real-world phenomena involve multiple interacting factors. Multiple Linear Regression extends the simple linear model to include multiple independent variables, enabling more comprehensive modeling and improved predictive power. Formally, the MLR model is expressed as:

$$Y = \beta_0 + \sum_{i=1}^{N_p} \beta_i X_i + \epsilon \tag{20}$$

where $Y$ is the dependent variable, $X_i$ are the $N_p$ independent variables (or combinations/polynomial expansions of independent variables), the $\beta_i$ are the regression coefficients, $\beta_0$ is the intercept of the model and $\epsilon$ is the error term.

Writing Eq. (20) in matrix form allows for the determination of the regression coefficients $\beta_i$:

$$\mathbf{Y} = \boldsymbol{\beta}\mathbf{X} + \boldsymbol{\epsilon} \tag{21}$$

**Table 4**
Number of significant harmonics $N_H$ for the regression models.

| Regression name | Speed (kn) | $N_H$ |
|---|---|---|
| Real heave $Re(\zeta)$ | 10.0 | 8 |
| | 12.5 | 8 |
| | 15.0 | 8 |
| | 17.5 | 9 |
| | 20.0 | 9 |
| Imaginary heave $Im(\zeta)$ | 10.0 | 20 |
| | 12.5 | 20 |
| | 15.0 | 20 |
| | 17.5 | 22 |
| | 20.0 | 22 |
| Real pitch $Re(\theta)$ | 10.0 | 7 |
| | 12.5 | 7 |
| | 15.0 | 7 |
| | 17.5 | 7 |
| | 20.0 | 8 |
| Imaginary pitch $Im(\theta)$ | 10.0 | 6 |
| | 12.5 | 6 |
| | 15.0 | 6 |
| | 17.5 | 6 |
| | 20.0 | 7 |

In Eq. (21), $\mathbf{Y}$ represents the matrix of observed data (the dependent variable), $\mathbf{X}$ is the matrix of independent variables, $\boldsymbol{\beta}$ is the matrix of regression coefficients and $\boldsymbol{\epsilon}$ is the matrix of errors. Employing this matrix form, the coefficients $\boldsymbol{\beta}$ result from:

$$\boldsymbol{\beta} = (\mathbf{X}'\mathbf{X})^{-1}\mathbf{X}'\mathbf{Y} \tag{22}$$

where $\mathbf{X}'$ is the transpose of $\mathbf{X}$ and $\mathbf{X}'\mathbf{X}$ is the inverse of $\mathbf{X}'\mathbf{X}$.

The present work considers four independent variables for the vertical motions fitting. The variables are the ones employed for developing the design space through the design of experiment technique previously described in Section 3.1. To recall, the independent variables are:

- Length to breadth ratio $L/B$.
- Breadth to draugth ratio $B/T$.
- Midship coefficient $C_X$.
- Prismatic coefficient $C_P$.

To achieve better fitting performances, it has be decided to employ a polynomial expansion of the independent variables up to a complete 2nd-order polynomial. To reduce the necessary amount of regressors, an automatic process is employed removing the unnecessary terms from the regressions according to the relative $p$-value and to the impact of the term on the determination coefficient $R^2$.

This technique has been employed for all the harmonics regressions, resulting in a total of 42 models for the real heave, 104 models for the imaginary heave, 36 models for the real pitch and 31 models for the imaginary pitch. To properly asses the quality of the obtained regressions, besides the $R^2$ coefficient described by Eq. (16), the following additional quality of fit indicators have been employed (Rinauro et al., 2024): the adjusted $R^2$ ($R^2_{adj}$), the Mean Absolute Percentage Error (MAPE), the Root Mean Square Error (RMSE), the Relative Root Mean Square Error (RRMSE) and the Pearson coefficient ($Prs$). The quality of fit indicators are defined as follows:

$$R^2_{adj} = 1 - (1 - R^2)\frac{n-1}{n-N_P-1} \tag{23}$$

$$\text{MAPE} = \frac{1}{n}\sum_{i=1}^{n}|y_i - y_i^*| \tag{24}$$

$$\text{RMSE} = \sqrt{\frac{1}{n}\sum_{i=1}^{n}(y_i - y_i^*)^2} \tag{25}$$

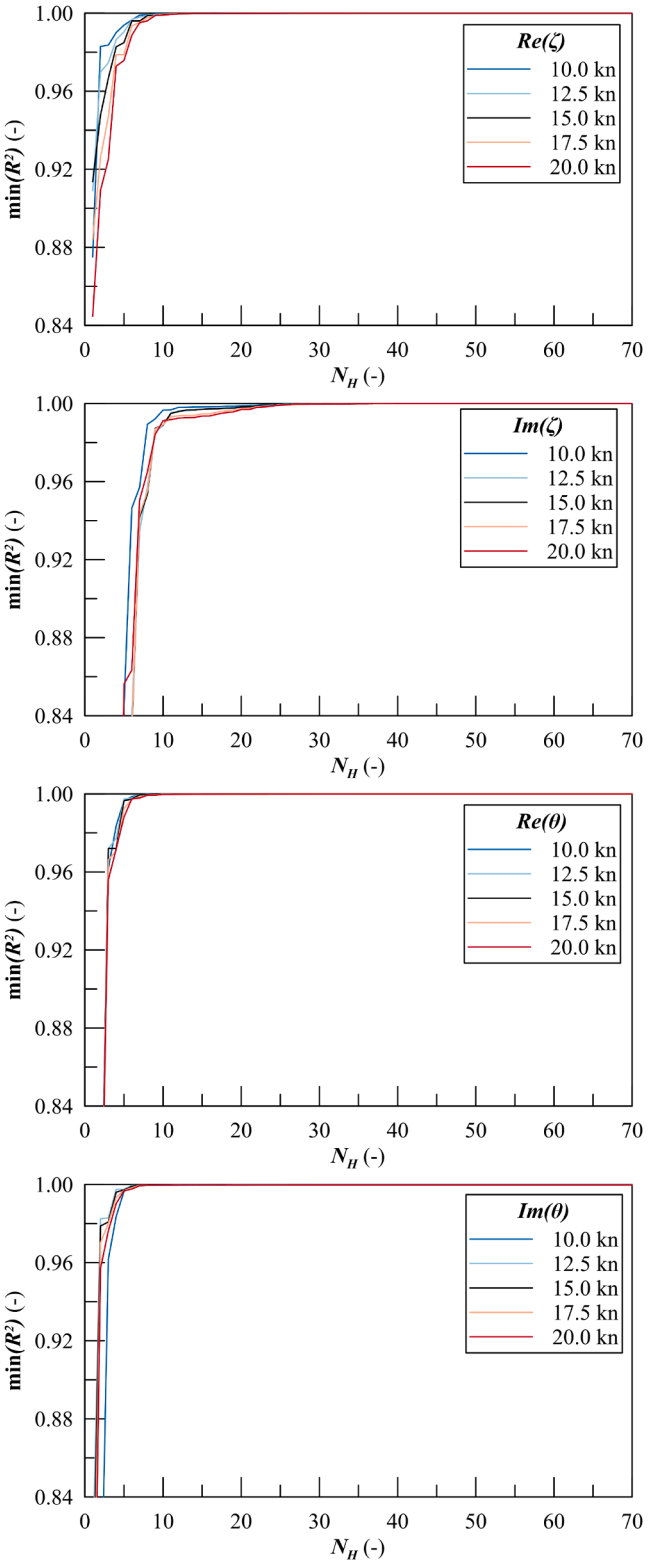


**Fig. 7.** $\min(R^2)$ values for the Fourier polynomial fitting.

$$\text{RRMSE} = \sqrt{\frac{\frac{1}{n}\sum_{i=1}^{n}(y_i - y_i^*)^2}{\sum_{i=1}^{n}(y_i^*)^2}} \tag{26}$$

$$Prs = \frac{\sum_{i=1}^{n}(y_i - \bar{y})(y_i - \bar{y^*})}{\sqrt{\sum_{i=1}^{n}(y_i - \bar{y})^2}\sqrt{\sum_{i=1}^{n}(y_i^* - \bar{y^*})^2}} \tag{27}$$

**Table 5**
Quality of fit indicators for the real heave transfer functions.

| | $a_0$ | $a_1$ | $a_2$ | $a_3$ | $a_4$ | $a_5$ | $a_6$ | $a_7$ | $a_8$ |
|---|---|---|---|---|---|---|---|---|---|
| | $V_s = 10.0$ kn | | | | | | | | |
| $R^2$ | 0.702 | 0.664 | 0.647 | 0.914 | 0.913 | 0.478 | 0.942 | 0.848 | – |
| $R^2_{adj}$ | 0.621 | 0.573 | 0.551 | 0.891 | 0.904 | 0.423 | 0.933 | 0.813 | – |
| MAPE | 0.028 | 0.009 | 0.099 | 0.248 | 0.064 | 0.111 | 0.027 | 0.106 | – |
| RMSE | 0.014 | 0.006 | 0.016 | 0.003 | 0.002 | 0.004 | 0.002 | 0.001 | – |
| RRMSE | 0.003 | 0.001 | 0.006 | 0.003 | 0.002 | 0.003 | 0.003 | 0.002 | – |
| $Prs$ | 0.838 | 0.815 | 0.804 | 0.956 | 0.955 | 0.691 | 0.971 | 0.921 | – |
| | $V_s = 12.5$ kn | | | | | | | | |
| $R^2$ | 0.690 | 0.699 | 0.644 | 0.846 | 0.835 | 0.597 | 0.953 | 0.804 | – |
| $R^2_{adj}$ | 0.606 | 0.629 | 0.547 | 0.810 | 0.803 | 0.530 | 0.947 | 0.743 | – |
| MAPE | 0.023 | 0.010 | 0.098 | 0.125 | 0.098 | 0.105 | 0.071 | 0.079 | – |
| RMSE | 0.012 | 0.007 | 0.012 | 0.005 | 0.004 | 0.004 | 0.002 | 0.001 | – |
| RRMSE | 0.002 | 0.001 | 0.005 | 0.003 | 0.003 | 0.003 | 0.002 | 0.001 | – |
| $Prs$ | 0.831 | 0.836 | 0.802 | 0.920 | 0.914 | 0.772 | 0.976 | 0.897 | – |
| | $V_s = 15.0$ kn | | | | | | | | |
| $R^2$ | 0.663 | 0.773 | 0.721 | 0.847 | 0.937 | 0.928 | 0.954 | 0.978 | – |
| $R^2_{adj}$ | 0.571 | 0.719 | 0.645 | 0.811 | 0.917 | 0.906 | 0.943 | 0.970 | – |
| MAPE | 0.020 | 0.009 | 0.067 | 0.082 | 0.074 | 0.061 | 0.059 | 0.065 | – |
| RMSE | 0.011 | 0.007 | 0.008 | 0.005 | 0.004 | 0.002 | 0.002 | 0.001 | – |
| RRMSE | 0.002 | 0.001 | 0.003 | 0.003 | 0.002 | 0.001 | 0.001 | 0.001 | – |
| $Prs$ | 0.814 | 0.879 | 0.849 | 0.920 | 0.968 | 0.963 | 0.976 | 0.988 | – |
| | $V_s = 17.5$ kn | | | | | | | | |
| $R^2$ | 0.649 | 0.803 | 0.915 | 0.833 | 0.940 | 0.988 | 0.945 | 0.993 | 0.951 |
| $R^2_{adj}$ | 0.554 | 0.749 | 0.896 | 0.794 | 0.927 | 0.985 | 0.936 | 0.991 | 0.936 |
| MAPE | 0.017 | 0.010 | 0.038 | 0.054 | 0.067 | 0.032 | 0.045 | 0.005 | 0.054 |
| RMSE | 0.010 | 0.007 | 0.005 | 0.005 | 0.005 | 0.001 | 0.003 | 0.001 | 0.001 |
| RRMSE | 0.002 | 0.001 | 0.002 | 0.002 | 0.003 | 0.001 | 0.001 | 0.002 | 0.001 |
| $Prs$ | 0.806 | 0.896 | 0.957 | 0.912 | 0.970 | 0.994 | 0.972 | 0.996 | 0.975 |
| | $V_s = 20.0$ kn | | | | | | | | |
| $R^2$ | 0.712 | 0.725 | 0.989 | 0.832 | 0.939 | 0.992 | 0.930 | 0.990 | 0.972 |
| $R^2_{adj}$ | 0.633 | 0.660 | 0.985 | 0.793 | 0.926 | 0.989 | 0.909 | 0.988 | 0.959 |
| MAPE | 0.013 | 0.010 | 0.014 | 0.039 | 0.050 | 2.864 | 0.033 | 0.015 | 0.040 |
| RMSE | 0.007 | 0.008 | 0.002 | 0.004 | 0.006 | 0.002 | 0.002 | 0.001 | 0.001 |
| RRMSE | 0.001 | 0.001 | 0.001 | 0.002 | 0.003 | 0.003 | 0.001 | 0.002 | 0.001 |
| $Prs$ | 0.843 | 0.851 | 0.994 | 0.912 | 0.969 | 0.996 | 0.964 | 0.995 | 0.986 |

where $n$ is the number of data points, $N_P$ is the number of predictors, $y_i$ are the predicted values, $\bar{y}$ is the mean of the predicted values, $y_i^*$ are the observed datapoints and $\bar{y^*}$ is the mean of the observed datapoints.

For evaluating the regressions according to the selected quality of fit indicators, it has to be set in mind that attributes like $R^2$, $R^2_{adj}$ and $Prs$ have to be maximised to obtain a good correlation. On the contrary, MAPE, RMSE and RRMSE have to be minimised. It has also to be considered that MAPE, RMSE and RRMSE are indicators whose magnitude is influenced by the variable values, while $R^2$, $R^2_{adj}$ and $Prs$ are absolute values in $[0, 1]$. For such a reason, it is easier to comment the results making reference to $R^2$, $R^2_{adj}$ and $Prs$ coefficients. In any case, fore completeness of the study, also the MAPE, RMSE and RRMSE are reported in the results.

Performing the quality of fit analysis on the regression sets of the study, the following considerations can be figured out:

- *Real heave* $Re(\zeta)$: Table 5 reports the quality of fit indicators for the harmonics $a_i$ representing the real heave transfer functions at the five calculation speeds. The models have a maximum of 9 harmonics $a_i$ for the speeds of 17.5 and 20.0 knots, the remaining speeds have 8 harmonics. The quality of fit indicators are different for each harmonics and speed; however, some trends can be identified. For the mean value $a_0$ the $R^2$ and $R^2_{adj}$ ranges from 0.554 to 0.712, indicating that the regression is moderate significant for the selected harmonics. The fact that there is a not excellent correlation between $a_0$ and the independent variables of the model may generate a shift in the mean value of $Re(\zeta)$ in the predicted surrogate TRF. For the other harmonics, the fitting quality is higher, except for the $a_5$ at the speed of 10.0 knots, where the quality of fit indicators identify a not satisfactory correlation with the independent variables. By increasing the speed there is a global trend in increasing the quality of fit level for the higher order harmonics, reaching really good correlation values. Even though quality of fit indicators like $R^2$ and $R^2_{adj}$ indicate moderate to low moderate correlations for certain harmonics, the $Prs$ coefficient remains quite high for all the $a_i$. As an example, $Prs$ value reaches a minimum of 0.691 for $a_5$ at 10.0 knots, when $R^2$ and $R^2_{adj}$ are close to 0.450. The fact that $Prs$ still indicates a reasonable correlation between all the harmonics and the independent variables gives confidence for a reasonably good reproduction of the $Re(\zeta)$ curves.
- *Imaginary heave* $Im(\zeta)$: Table 6 reports the quality of fit indicators for the harmonics $a_i$ representing the imaginary heave transfer functions at the five calculation speeds. $Im(\zeta)$ is the complex TRF part requiring the higher number of harmonics $a_i$ at each speed, dealing with numbers ranging from 20 to 22. The quality of fit indicators show different fitting quality for each harmonics, with different trends compared to the ones observed for $Re(\zeta)$. Starting with the mean value $a_0$ of the model, here the indicators show a quite high fitting level. The $R^2$ and $R^2_{adj}$ values are quite high, ranging from 0.887 up to 0.970. However, the trend is opposite compared to $Re(\zeta)$, as the quality of fit decrease with the speed. In fact the higher values for the indicators are for the speed of 10.0 knots and the worse for the speed of 20.0 knots. The first harmonic $a_1$ shows a moderate correlation with the independent variables for the speeds of 10.0 and 12.5 knots. The correlation is good for the remaining speeds. For the remaining harmonics, a good correlation can be observed at the speeds of 15.0, 17.5 and 20.0 knots, observing $R^2$ and $R^2_{adj}$ values always above 0.800. At the speeds of 10.0 and 12.5 a moderate correlation is observed for the harmonics $a_3$, $a_4$, $a_{14}$ and $a_{16}$. Considering only the speed of 10.0 knots, also the harmonics $a_{13}$ and $a_6$ have a moderate correlation. In any case, the worse correlation is observed for $a_1$ at the speed of 12.5 knots, having a $R^2_{adj}$ of 0.452. It is not possible to define a global trend among the models at different speeds; however, as a general indication, it appears that $Im(\zeta)$ is well reproduced for the higher speed, while some problems may appear at the lower speed. As the intercept $a_0$ is well reproduced for all the speeds, it is reasonable to suppose that $Im(\zeta)$ will be not affected by a shift in the mean value as it is for $Re(\zeta)$. Taking a look to the general shape of the $Im(\zeta)$ in Fig. 5, it is observed that the curves have a wider oscillation compared to the other complex TRF parts, therefore, the reproduction of the peaks may be affected by the moderate correlation of certain harmonics. In any case, also for $Im(\zeta)$ the level of the $Prs$ coefficient remains significantly high for all the $a_i$, reaching a minimum of 0.737 for $a_1$ at 10.0 knots. Therefore, it is reasonable that the provided models could reproduce quite well the $Im(\zeta)$ curves.
- *Real pitch* $Re(\theta)$: Table 7 reports the quality of fit indicators for the harmonics $a_i$ representing the real pitch transfer functions at the five calculation speeds. The reproduction of $Re(\theta)$ requires a lower amount of harmonics compared to the complex heave parts. 7 harmonics are necessaries for the speeds of 10.0, 12.5, 15.0 and 15.0 knots and 8 for the speed of 20.0 knots. Considering the mean value of the model $a_0$, the correlations found are moderate for all the speed range considered in the analysis. The values shown in Table 7 highlights $R^2$ and $R^2_{adj}$ ranging between 0.579 and 0.690. There is no general trend between the different speed, as the quality of fit indicators oscillates among the calculated velocities. Also for the first harmonic $a_1$ there is a moderate correlation with the independent variables, with values for $R^2$ and $R^2_{adj}$ ranging between 0.545 and 0.731. In this case, there is a trend with the speed, with the higher correlation values at the higher speeds. The remaining harmonics reach a quite good correlation level at all the speeds, showing, in general, a better correlation at the high speeds. As a general indication, $Re(\theta)$ has the

**Table 6**
Quality of fit indicators for the imaginary heave transfer functions.

| | $a_0$ | $a_1$ | $a_2$ | $a_3$ | $a_4$ | $a_5$ | $a_6$ | $a_7$ | $a_8$ | $a_9$ | $a_{10}$ | $a_{11}$ | $a_{12}$ | $a_{13}$ | $a_{14}$ | $a_{15}$ | $a_{16}$ | $a_{17}$ | $a_{18}$ | $a_{19}$ | $a_{20}$ | $a_{21}$ |
|---|---|---|---|---|---|---|---|---|---|---|---|---|---|---|---|---|---|---|---|---|---|---|
| | $V_s = 10.0$ kn | | | | | | | | | | | | | | | | | | | | | |
| $R^2$ | 0.970 | 0.670 | 0.874 | 0.765 | 0.762 | 0.992 | 0.578 | 0.945 | 0.936 | 0.958 | 0.919 | 0.798 | 0.929 | 0.679 | 0.558 | 0.631 | 0.665 | 0.730 | 0.892 | 0.712 | - | - |
| $R^2_{adj}$ | 0.962 | 0.593 | 0.849 | 0.723 | 0.697 | 0.990 | 0.507 | 0.934 | 0.919 | 0.939 | 0.906 | 0.704 | 0.910 | 0.636 | 0.470 | 0.557 | 0.587 | 0.666 | 0.858 | 0.633 | - | - |
| MAPE | 0.018 | 0.003 | 0.060 | 0.039 | 0.230 | 0.055 | 0.095 | 0.906 | 0.090 | 0.076 | 0.001 | 0.114 | 1.394 | 0.024 | 0.566 | 0.103 | 0.146 | 0.932 | 0.156 | 0.044 | - | - |
| RMSE | 0.002 | 0.004 | 0.006 | 0.003 | 0.005 | 0.001 | 0.003 | 0.001 | 0.001 | 0.001 | 0.001 | 0.001 | 0.001 | 0.001 | 0.001 | 0.001 | 0.001 | 0.001 | 0.001 | 0.001 | - | - |
| RRMSE | 0.001 | 0.004 | 0.003 | 0.002 | 0.004 | 0.001 | 0.002 | 0.004 | 0.001 | 0.001 | 0.003 | 0.002 | 0.001 | 0.003 | 0.003 | 0.001 | 0.004 | 0.001 | 0.001 | 0.028 | - | - |
| *Prs* | 0.985 | 0.819 | 0.935 | 0.877 | 0.873 | 0.996 | 0.760 | 0.972 | 0.967 | 0.978 | 0.958 | 0.893 | 0.964 | 0.824 | 0.747 | 0.794 | 0.815 | 0.854 | 0.944 | 0.843 | - | - |
| | $V_s = 12.5$ kn | | | | | | | | | | | | | | | | | | | | | |
| $R^2$ | 0.935 | 0.544 | 0.871 | 0.762 | 0.774 | 0.946 | 0.588 | 0.969 | 0.865 | 0.974 | 0.963 | 0.971 | 0.865 | 0.947 | 0.697 | 0.904 | 0.700 | 0.880 | 0.812 | 0.848 | - | - |
| $R^2_{adj}$ | 0.926 | 0.452 | 0.840 | 0.730 | 0.721 | 0.935 | 0.520 | 0.965 | 0.811 | 0.967 | 0.950 | 0.958 | 0.829 | 0.926 | 0.665 | 0.874 | 0.650 | 0.856 | 0.787 | 0.801 | - | - |
| MAPE | 0.095 | 0.278 | 0.182 | 0.034 | 0.166 | 0.060 | 0.093 | 0.172 | 0.075 | 0.013 | 0.072 | 0.257 | 0.229 | 0.226 | 0.293 | 0.094 | 0.056 | 0.259 | 0.036 | 0.325 | - | - |
| RMSE | 0.004 | 0.004 | 0.009 | 0.002 | 0.005 | 0.002 | 0.003 | 0.001 | 0.001 | 0.001 | 0.001 | 0.001 | 0.001 | 0.000 | 0.000 | 0.000 | 0.000 | 0.000 | 0.000 | 0.000 | - | - |
| RRMSE | 0.002 | 0.006 | 0.005 | 0.001 | 0.004 | 0.002 | 0.002 | 0.002 | 0.001 | 0.003 | 0.001 | 0.002 | 0.001 | 0.001 | 0.002 | 0.001 | 0.003 | 0.001 | 0.004 | 0.001 | - | - |
| *Prs* | 0.967 | 0.737 | 0.933 | 0.873 | 0.880 | 0.972 | 0.767 | 0.984 | 0.930 | 0.987 | 0.981 | 0.985 | 0.930 | 0.973 | 0.835 | 0.951 | 0.836 | 0.938 | 0.901 | 0.921 | - | - |
| | $V_s = 15.0$ kn | | | | | | | | | | | | | | | | | | | | | |
| $R^2$ | 0.933 | 0.955 | 0.867 | 0.948 | 0.840 | 0.947 | 0.963 | 0.965 | 0.979 | 0.962 | 0.985 | 0.960 | 0.988 | 0.941 | 0.902 | 0.944 | 0.864 | 0.940 | 0.944 | 0.950 | - | - |
| $R^2_{adj}$ | 0.918 | 0.941 | 0.836 | 0.932 | 0.796 | 0.935 | 0.950 | 0.959 | 0.971 | 0.956 | 0.979 | 0.953 | 0.984 | 0.930 | 0.879 | 0.932 | 0.832 | 0.926 | 0.924 | 0.932 | - | - |
| MAPE | 0.219 | 0.113 | 0.749 | 0.038 | 0.096 | 0.056 | 0.062 | 0.111 | 0.004 | 0.082 | 0.058 | 0.348 | 0.058 | 0.138 | 0.116 | 0.040 | 0.092 | 0.108 | 0.198 | 0.108 | - | - |
| RMSE | 0.005 | 0.001 | 0.010 | 0.003 | 0.004 | 0.003 | 0.001 | 0.002 | 0.001 | 0.001 | 0.000 | 0.001 | 0.000 | 0.000 | 0.000 | 0.000 | 0.000 | 0.000 | 0.000 | 0.000 | - | - |
| RRMSE | 0.004 | 0.001 | 0.031 | 0.001 | 0.003 | 0.002 | 0.001 | 0.001 | 0.001 | 0.001 | 0.001 | 0.001 | 0.000 | 0.002 | 0.001 | 0.006 | 0.001 | 0.002 | 0.002 | 0.000 | - | - |
| *Prs* | 0.966 | 0.977 | 0.931 | 0.974 | 0.916 | 0.973 | 0.981 | 0.982 | 0.989 | 0.981 | 0.992 | 0.979 | 0.994 | 0.970 | 0.949 | 0.971 | 0.929 | 0.969 | 0.971 | 0.974 | - | - |
| | $V_s = 17.5$ kn | | | | | | | | | | | | | | | | | | | | | |
| $R^2$ | 0.911 | 0.949 | 0.854 | 0.953 | 0.928 | 0.942 | 0.992 | 0.949 | 0.990 | 0.933 | 0.988 | 0.907 | 0.940 | 0.912 | 0.750 | 0.957 | 0.825 | 0.975 | 0.973 | 0.974 | 0.979 | 0.903 |
| $R^2_{adj}$ | 0.890 | 0.931 | 0.814 | 0.938 | 0.905 | 0.932 | 0.990 | 0.933 | 0.987 | 0.912 | 0.986 | 0.878 | 0.930 | 0.881 | 0.716 | 0.946 | 0.796 | 0.968 | 0.966 | 0.967 | 0.973 | 0.884 |
| MAPE | 0.157 | 0.102 | 0.169 | 0.047 | 0.059 | 0.045 | 0.400 | 0.046 | 0.085 | 0.061 | 0.067 | 0.169 | 0.894 | 0.141 | 0.696 | 0.129 | 0.022 | 0.401 | 3.310 | 0.062 | 0.121 | 0.164 |
| RMSE | 0.006 | 0.003 | 0.010 | 0.005 | 0.003 | 0.004 | 0.001 | 0.002 | 0.001 | 0.001 | 0.000 | 0.000 | 0.000 | 0.000 | 0.000 | 0.000 | 0.000 | 0.000 | 0.000 | 0.000 | 0.000 | 0.000 |
| RRMSE | 0.009 | 0.002 | 0.007 | 0.002 | 0.002 | 0.002 | 0.001 | 0.001 | 0.003 | 0.001 | 0.002 | 0.001 | 0.010 | 0.001 | 0.009 | 0.001 | 0.005 | 0.001 | 0.001 | 0.001 | 0.001 | 0.000 |
| *Prs* | 0.954 | 0.974 | 0.924 | 0.976 | 0.963 | 0.970 | 0.996 | 0.974 | 0.995 | 0.965 | 0.994 | 0.952 | 0.969 | 0.955 | 0.866 | 0.978 | 0.908 | 0.987 | 0.986 | 0.987 | 0.989 | 0.950 |
| | $V_s = 20.0$ kn | | | | | | | | | | | | | | | | | | | | | |
| $R^2$ | 0.909 | 0.939 | 0.833 | 0.943 | 0.983 | 0.924 | 0.990 | 0.920 | 0.991 | 0.986 | 0.987 | 0.989 | 0.965 | 0.984 | 0.931 | 0.863 | 0.842 | 0.824 | 0.769 | 0.901 | 0.827 | 0.946 |
| $R^2_{adj}$ | 0.887 | 0.920 | 0.787 | 0.928 | 0.979 | 0.911 | 0.987 | 0.895 | 0.989 | 0.980 | 0.984 | 0.985 | 0.958 | 0.978 | 0.917 | 0.815 | 0.816 | 0.789 | 0.731 | 0.874 | 0.798 | 0.937 |
| MAPE | 0.166 | 0.090 | 0.111 | 0.049 | 0.484 | 0.043 | 0.036 | 0.037 | 36.82 | 0.057 | 0.083 | 0.025 | 0.141 | 0.268 | 0.187 | 0.186 | 3.463 | 0.616 | 0.026 | 0.173 | 0.171 | 0.410 |
| RMSE | 0.007 | 0.004 | 0.010 | 0.007 | 0.002 | 0.004 | 0.002 | 0.001 | 0.001 | 0.000 | 0.000 | 0.000 | 0.000 | 0.000 | 0.000 | 0.000 | 0.000 | 0.000 | 0.000 | 0.000 | 0.000 | 0.000 |
| RRMSE | 0.005 | 0.002 | 0.005 | 0.002 | 0.001 | 0.002 | 0.003 | 0.001 | 0.001 | 0.000 | 0.001 | 0.001 | 0.001 | 0.001 | 0.001 | 0.001 | 0.002 | 0.001 | 0.002 | 0.001 | 0.002 | 0.000 |
| *Prs* | 0.953 | 0.969 | 0.912 | 0.971 | 0.991 | 0.961 | 0.995 | 0.959 | 0.995 | 0.993 | 0.993 | 0.994 | 0.982 | 0.992 | 0.964 | 0.929 | 0.917 | 0.907 | 0.877 | 0.949 | 0.909 | 0.972 |

same issues highlighted for $Re(\theta)$, means a problem in the reproduction of the mean level of the curves, possibly resulting in a shift of the surrogate TRFs. In any case, also for $Re(\theta)$, the $Prs$ correlation coefficient remains high for all the fitted harmonics, ranging from 0.801 (for $a_1$ at 10.0 knots) up to 0.993 (for $a_6$ at 17.5 knots). Such a matter gives sufficient confidence that the provided surrogate model can reasonably good reproduce $Re(\theta)$ at all the considered speeds.

- *Imaginary pitch* $Im(\theta)$: Table 8 reports the quality of fit indicators for the harmonics $a_i$ representing the imaginary pitch transfer functions at the five calculation speeds. $Im(\theta)$ is the complex TRF part that necessitates the lower number of harmonics $a_i$ to be reproduced, requiring 7 harmonics for the speeds of 10.0, 12.5, 15.0 and 17.5 knots and 6 harmonics for the speed of 20.0 knots. Considering the mean value $a_0$, the correlation obtained with the independent variable is moderate for all the speeds. The $R^2$ and $R^2_{adj}$ values ranges from 0.515 up to 0.732, highlighting higher correlation values for the speeds of 17.5 and 20.0 knots. Also the first harmonic $a_1$ has a moderate significant correlation, with values of $R^2$ and $R^2_{adj}$ ranging from 0.515 to 0.693. For the speed of 10.0 knots also $a_3$ shows a moderate significant correlation with the independent variables, while for the remaining harmonics all the correlations are quite good considering all the speed range. Also in this case, as for $Re(\zeta)$ and $Re(\theta)$, the moderate correlation of the mean value $a_0$ may generate a shift in the reproduction of the surrogate curves. However, for all harmonics and speeds the level of the $Prs$ coefficient remains quite high, ranging from 0.786 to 0.989. This gives a confidence that also $Im(\theta)$ could be well reproduced by the provided surrogate model.

Dealing with a consistent number of regressions (a total of 213 models), the coefficients and the polynomial form of the resulting MLR models is not reported directly in the paper. A supplementary file is provided, including all the regressions coefficients, the relative $p$-values and other statistical information.

The present section presented the quality of fit obtained for each harmonic $a_i$ for the TRFs models at different speeds. However, it is hard to judge how the resulting TRFs are reproduced taking a look only at the quality of fit indicators. Therefore, it is necessary to verify the models by comparing directly the surrogate TRFs with the original ones, checking how the resulting curves match with each other. Such a process will be performed in the next section.

## 5. Model verification and application

The previous section presented the regressions on the harmonics needed to reproduce the real and imaginary part of heave and pitch transfer functions in head sea at different speeds. The quality of fit indicators reported in the study refer to the individual harmonics; therefore, for practical purposes, there is the need for verifying the effective reproduction of the transfer functions.

The verification process is performed in two steps:

- Transfer functions reproduction of the 25 vessels composing the initial database.
- Application of the regressions to a ship external to the initial database, with evaluation of the $CR_V$ indices and comparison with direct numerical results.

**Table 7**
Quality of fit indicators for real pitch transfer functions.

| | $a_0$ | $a_1$ | $a_2$ | $a_3$ | $a_4$ | $a_5$ | $a_6$ | $a_7$ |
|---|---|---|---|---|---|---|---|---|
| | $V_s = 10.0$ kn | | | | | | | |
| $R^2$ | 0.669 | 0.642 | 0.909 | 0.860 | 0.813 | 0.956 | 0.898 | – |
| $R^2_{adj}$ | 0.579 | 0.545 | 0.894 | 0.832 | 0.769 | 0.951 | 0.877 | – |
| MAPE | 0.046 | 0.045 | 0.026 | 0.031 | 0.077 | 0.046 | 0.055 | – |
| RMSE | 0.011 | 0.013 | 0.002 | 0.004 | 0.002 | 0.001 | 0.001 | – |
| RRMSE | 0.003 | 0.003 | 0.001 | 0.001 | 0.002 | 0.001 | 0.001 | – |
| $Prs$ | 0.818 | 0.801 | 0.953 | 0.927 | 0.901 | 0.978 | 0.947 | – |
| | $V_s = 12.5$ kn | | | | | | | |
| $R^2$ | 0.682 | 0.672 | 0.858 | 0.894 | 0.876 | 0.936 | 0.976 | – |
| $R^2_{adj}$ | 0.595 | 0.583 | 0.830 | 0.873 | 0.846 | 0.923 | 0.970 | – |
| MAPE | 0.037 | 0.039 | 0.041 | 0.026 | 0.164 | 0.036 | 0.079 | – |
| RMSE | 0.010 | 0.012 | 0.003 | 0.004 | 0.003 | 0.001 | 0.001 | – |
| RRMSE | 0.003 | 0.003 | 0.002 | 0.001 | 0.004 | 0.001 | 0.001 | – |
| $Prs$ | 0.825 | 0.820 | 0.926 | 0.945 | 0.935 | 0.967 | 0.987 | – |
| | $V_s = 15.0$ kn | | | | | | | |
| $R^2$ | 0.681 | 0.706 | 0.839 | 0.920 | 0.916 | 0.944 | 0.985 | – |
| $R^2_{adj}$ | 0.594 | 0.626 | 0.813 | 0.906 | 0.897 | 0.929 | 0.982 | – |
| MAPE | 0.031 | 0.034 | 0.060 | 0.020 | 0.002 | 0.024 | 0.090 | – |
| RMSE | 0.009 | 0.012 | 0.004 | 0.003 | 0.003 | 0.001 | 0.001 | – |
| RRMSE | 0.002 | 0.003 | 0.002 | 0.001 | 0.006 | 0.001 | 0.002 | – |
| $Prs$ | 0.825 | 0.840 | 0.916 | 0.959 | 0.957 | 0.971 | 0.992 | – |
| | $V_s = 17.5$ kn | | | | | | | |
| $R^2$ | 0.690 | 0.723 | 0.838 | 0.921 | 0.934 | 0.744 | 0.987 | – |
| $R^2_{adj}$ | 0.606 | 0.648 | 0.806 | 0.908 | 0.918 | 0.674 | 0.985 | – |
| MAPE | 0.026 | 0.030 | 0.130 | 0.016 | 0.136 | 0.037 | 0.075 | – |
| RMSE | 0.008 | 0.011 | 0.005 | 0.002 | 0.003 | 0.001 | 0.001 | – |
| RRMSE | 0.002 | 0.002 | 0.004 | 0.001 | 0.003 | 0.001 | 0.001 | – |
| $Prs$ | 0.831 | 0.850 | 0.915 | 0.960 | 0.966 | 0.862 | 0.993 | – |
| | $V_s = 20.0$ kn | | | | | | | |
| $R^2$ | 0.682 | 0.731 | 0.859 | 0.919 | 0.946 | 0.766 | 0.983 | 0.964 |
| $R^2_{adj}$ | 0.607 | 0.658 | 0.826 | 0.900 | 0.934 | 0.702 | 0.977 | 0.955 |
| MAPE | 0.021 | 0.026 | 0.074 | 0.013 | 0.092 | 0.061 | 0.048 | 0.015 |
| RMSE | 0.007 | 0.010 | 0.005 | 0.002 | 0.003 | 0.002 | 0.001 | 0.001 |
| RRMSE | 0.002 | 0.002 | 0.006 | 0.001 | 0.00 | 0.001 | 0.001 | 0.001 |
| $Prs$ | 0.826 | 0.855 | 0.927 | 0.958 | 0.972 | 0.875 | 0.991 | 0.981 |

**Table 8**
Quality of fit indicators for imaginary pitch transfer functions.

| | $a_0$ | $a_1$ | $a_2$ | $a_3$ | $a_4$ | $a_5$ | $a_6$ |
|---|---|---|---|---|---|---|---|
| | $V_s = 10.0$ kn | | | | | | |
| $R^2$ | 0.677 | 0.619 | 0.802 | 0.712 | 0.959 | 0.976 | – |
| $R^2_{adj}$ | 0.589 | 0.515 | 0.756 | 0.633 | 0.955 | 0.968 | – |
| MAPE | 0.016 | 0.013 | 0.028 | 0.126 | 0.037 | 0.022 | – |
| RMSE | 0.008 | 0.010 | 0.006 | 0.005 | 0.001 | 0.001 | – |
| RRMSE | 0.001 | 0.001 | 0.002 | 0.004 | 0.001 | 0.001 | – |
| $Prs$ | 0.823 | 0.787 | 0.896 | 0.843 | 0.979 | 0.987 | – |
| | $V_s = 12.5$ kn | | | | | | |
| $R^2$ | 0.693 | 0.619 | 0.833 | 0.757 | 0.963 | 0.973 | – |
| $R^2_{adj}$ | 0.610 | 0.515 | 0.793 | 0.690 | 0.958 | 0.967 | – |
| MAPE | 0.018 | 0.015 | 0.025 | 0.675 | 0.027 | 0.129 | – |
| RMSE | 0.008 | 0.011 | 0.006 | 0.006 | 0.001 | 0.001 | – |
| RRMSE | 0.002 | 0.002 | 0.002 | 0.006 | 0.001 | 0.001 | – |
| $Prs$ | 0.832 | 0.786 | 0.912 | 0.870 | 0.981 | 0.986 | – |
| | $V_s = 15.0$ kn | | | | | | |
| $R^2$ | 0.717 | 0.644 | 0.868 | 0.778 | 0.950 | 0.977 | – |
| $R^2_{adj}$ | 0.640 | 0.548 | 0.837 | 0.726 | 0.936 | 0.973 | – |
| MAPE | 0.021 | 0.016 | 0.020 | 0.081 | 0.020 | 1.466 | – |
| RMSE | 0.009 | 0.011 | 0.005 | 0.007 | 0.001 | 0.001 | – |
| RRMSE | 0.002 | 0.002 | 0.001 | 0.016 | 0.001 | 0.008 | – |
| $Prs$ | 0.846 | 0.803 | 0.931 | 0.882 | 0.974 | 0.988 | – |
| | $V_s = 17.5$ kn | | | | | | |
| $R^2$ | 0.732 | 0.666 | 0.872 | 0.812 | 0.879 | 0.976 | – |
| $R^2_{adj}$ | 0.659 | 0.575 | 0.850 | 0.768 | 0.846 | 0.973 | – |
| MAPE | 0.023 | 0.018 | 0.017 | 0.070 | 0.026 | 0.303 | – |
| RMSE | 0.009 | 0.011 | 0.005 | 0.007 | 0.001 | 0.001 | – |
| RRMSE | 0.002 | 0.002 | 0.001 | 0.006 | 0.001 | 0.001 | – |
| $Prs$ | 0.855 | 0.816 | 0.933 | 0.901 | 0.937 | 0.988 | – |
| | $V_s = 20.0$ kn | | | | | | |
| $R^2$ | 0.731 | 0.693 | 0.893 | 0.862 | 0.770 | 0.978 | 0.937 |
| $R^2_{adj}$ | 0.658 | 0.610 | 0.876 | 0.824 | 0.717 | 0.976 | 0.920 |
| MAPE | 0.026 | 0.019 | 0.015 | 0.228 | 0.037 | 0.098 | 0.057 |
| RMSE | 0.010 | 0.012 | 0.004 | 0.007 | 0.002 | 0.001 | 0.001 |
| RRMSE | 0.002 | 0.002 | 0.001 | 0.004 | 0.001 | 0.001 | 0.001 |
| $Prs$ | 0.855 | 0.832 | 0.945 | 0.928 | 0.878 | 0.989 | 0.968 |

These two steps allow for ensuring the validity of the obtained regression and verify the generalisation of the methods for vessels having the main dimensions and parameters included in the database bounds. The following sections presents these two verification steps, reporting all the methods and results obtained by applying the proposed regressions set.

### 5.1. Original database reproduction

The first step of the models verification process consists in reproducing the real and imaginary part of heave and pitch transfer functions for the 25 vessels included in the initial database. The verification include all the five speeds considered in the analysis for the head sea conditions.

The quality evaluation process of the surrogate transfer functions is made through a direct comparison between original numerical curves and surrogate ones. The metric for quality is the $R^2$ determination coefficient, calculated according to Eq. (16). The surrogate real and imaginary part of heave and pitch have been calculated according to Eq. (15), employing a range for $\omega^*$ between 0.0 and 0.7 rad/s in steps of 0.01 rad/s, corresponding to a frequency range $\omega$ between 0.3 and 1.0. The comparison has been performed with the numerical complex transfer functions on the same frequency range.

Table 9 reports the quality of fit results for the complex transfer functions of heave, considering the five different speeds. Considering the real part of the transfer function $Re(\zeta)$, the quality of fit is high for all the speed range. At 10.0 knots, the worst $R^2$ is 0.986 (corresponding to Hull 02), with an average value of 0.997 among all the 25 vessels. Increasing the speed, the fitting quality is slightly increasing. At 12.5 knots, the average value is still about 0.997, but with a minimum of 0.989 (corresponding also in this case to Hull 02). At 15.0 knots the average $R^2$ is 0.997, registering a minimum of 0.991 for Hull 02. At 17.5 knots the average $R^2$ increases to 0.998, with a minimum of 0.994 always for Hull 02. Finally, for a speed of 20.0 knots, the average value is of 0.998, with a minimum of 0.995 for Hull 02. Considering the levels of the quality of fit indicators reported in Section 4, which were not extremely high for certain harmonics $a_i$, the global effect on the fitting of $Re(\zeta)$ is not affected by moderate correlations found in the single harmonics regressions. Therefore, the significance of the proposed model for $Re(\zeta)$ is extremely good for the database reproduction.

Considering the imaginary part of the transfer function $Im(\zeta)$, the global trends of the quality of fit indicators in Table 9 is lower than the values for $Re(\zeta)$. For the speed of 10.0 knots, the average value of $R^2$ is 0.989. The minimum in this case is of 0.942 (corresponding to Hull 24). For the speed of 12.5 knots, the average value decreases to 0.977, with a minimum of 0.884, also in this case corresponding to Hull 24. Increasing the speed to 15.0 knots, the average $R^2$ maintains the value of 0.977, with a minimum of 0.906, corresponding this time to Hull 02. At $V_s = 17.5$ knots, the corresponding $R^2$ is 0.984, with a minimum of 0.946 for Hull 24. Finally, for a speed of 20.0 knots, the average $R^2$ value is 0.989, with a minimum of 0.964 again for Hull 24. In this case, the worst values are not always corresponding to the same hull form (as it was for $Re(\zeta)$), but three different hulls are detected at different speeds. The level of the average quality of fit is still high, but less compared to $Re(\zeta)$, especially considering the minima at each speed. $Im(\zeta)$ is probably the most complicated function to fit as it requires a consistently higher amount of harmonics $a_i$ at each speed to be reproduced by the Fourier model (see Table 4). In any case, the levels of $R^2$ are all

**Table 9**
Data fitting of heave transfer functions on the original 25 hull forms.

| | $Re(\zeta)$ | | | | | $Im(\zeta)$ | | | | |
|---|---|---|---|---|---|---|---|---|---|---|
| | $V_s = 10.0$ kn | $V_s = 12.5$ kn | $V_s = 15.0$ kn | $V_s = 17.5$ kn | $V_s = 20.0$ kn | $V_s = 10.0$ kn | $V_s = 12.5$ kn | $V_s = 15.0$ kn | $V_s = 17.5$ kn | $V_s = 20.0$ kn |
| Hull 01 | 0.999 | 0.999 | 0.998 | 0.999 | 0.998 | 0.996 | 0.987 | 0.989 | 0.994 | 0.995 |
| Hull 02 | 0.986 | 0.989 | 0.991 | 0.994 | 0.995 | 0.974 | 0.918 | 0.906 | 0.948 | 0.966 |
| Hull 03 | 0.998 | 0.998 | 0.997 | 0.999 | 0.998 | 0.986 | 0.975 | 0.991 | 0.993 | 0.993 |
| Hull 04 | 0.998 | 0.997 | 0.996 | 0.998 | 0.996 | 0.948 | 0.913 | 0.998 | 0.997 | 0.999 |
| Hull 05 | 0.999 | 0.998 | 0.996 | 0.997 | 0.996 | 0.976 | 0.972 | 0.993 | 0.996 | 0.998 |
| Hull 06 | 0.996 | 0.997 | 0.997 | 0.998 | 0.998 | 0.992 | 0.973 | 0.942 | 0.969 | 0.980 |
| Hull 07 | 1.000 | 0.999 | 0.998 | 0.999 | 0.998 | 0.998 | 0.995 | 0.997 | 0.998 | 0.996 |
| Hull 08 | 0.999 | 0.999 | 0.999 | 0.999 | 0.999 | 0.999 | 0.995 | 0.996 | 0.998 | 0.998 |
| Hull 09 | 0.994 | 0.995 | 0.996 | 0.997 | 0.997 | 0.990 | 0.970 | 0.962 | 0.977 | 0.985 |
| Hull 10 | 0.994 | 0.995 | 0.996 | 0.997 | 0.998 | 0.991 | 0.969 | 0.955 | 0.971 | 0.980 |
| Hull 11 | 0.998 | 0.998 | 0.998 | 0.999 | 0.998 | 0.999 | 0.996 | 0.995 | 0.998 | 0.998 |
| Hull 12 | 0.997 | 0.997 | 0.997 | 0.998 | 0.997 | 0.999 | 0.993 | 0.995 | 0.995 | 0.995 |
| Hull 13 | 0.999 | 0.999 | 0.998 | 0.999 | 0.998 | 0.998 | 0.989 | 0.995 | 0.998 | 0.996 |
| Hull 14 | 0.997 | 0.997 | 0.997 | 0.998 | 0.998 | 0.996 | 0.990 | 0.964 | 0.954 | 0.968 |
| Hull 15 | 0.999 | 0.999 | 0.999 | 0.999 | 1.000 | 0.998 | 0.999 | 0.998 | 0.995 | 0.996 |
| Hull 16 | 0.999 | 0.999 | 0.999 | 0.999 | 0.999 | 0.999 | 0.998 | 0.996 | 0.997 | 0.998 |
| Hull 17 | 0.998 | 0.999 | 0.998 | 0.999 | 0.999 | 0.996 | 0.989 | 0.972 | 0.965 | 0.977 |
| Hull 18 | 0.999 | 0.999 | 0.997 | 0.998 | 0.998 | 0.985 | 0.989 | 0.996 | 0.998 | 0.997 |
| Hull 19 | 0.997 | 0.997 | 0.997 | 0.998 | 0.998 | 0.995 | 0.988 | 0.981 | 0.988 | 0.995 |
| Hull 20 | 0.999 | 0.999 | 0.998 | 0.999 | 0.997 | 0.994 | 0.986 | 0.986 | 0.994 | 0.996 |
| Hull 21 | 0.999 | 0.999 | 0.999 | 0.999 | 0.999 | 0.996 | 0.996 | 0.992 | 0.987 | 0.986 |
| Hull 22 | 0.997 | 0.998 | 0.998 | 0.999 | 0.999 | 0.995 | 0.989 | 0.993 | 0.987 | 0.992 |
| Hull 23 | 0.999 | 0.998 | 0.998 | 0.998 | 0.997 | 0.995 | 0.978 | 0.966 | 0.980 | 0.993 |
| Hull 24 | 0.987 | 0.990 | 0.993 | 0.995 | 0.996 | 0.942 | 0.884 | 0.908 | 0.946 | 0.964 |
| Hull 25 | 0.996 | 0.997 | 0.997 | 0.998 | 0.998 | 0.994 | 0.984 | 0.970 | 0.983 | 0.991 |
| min | 0.986 | 0.989 | 0.991 | 0.994 | 0.995 | 0.942 | 0.884 | 0.906 | 0.946 | 0.964 |
| max | 1.000 | 0.999 | 0.999 | 0.999 | 1.000 | 0.999 | 0.999 | 0.998 | 0.998 | 0.999 |
| mean | 0.997 | 0.997 | 0.997 | 0.998 | 0.998 | 0.989 | 0.977 | 0.977 | 0.984 | 0.989 |

**Table 10**
Data fitting of pitch transfer functions on the original 25 hull forms.

| | $Re(\theta)$ | | | | | $Im(\theta)$ | | | | |
|---|---|---|---|---|---|---|---|---|---|---|
| | $V_s = 10.0$ kn | $V_s = 12.5$ kn | $V_s = 15.0$ kn | $V_s = 17.5$ kn | $V_s = 20.0$ kn | $V_s = 10.0$ kn | $V_s = 12.5$ kn | $V_s = 15.0$ kn | $V_s = 17.5$ kn | $V_s = 20.0$ kn |
| Hull 01 | 0.998 | 0.998 | 0.998 | 0.998 | 0.999 | 0.999 | 0.998 | 0.998 | 0.997 | 0.998 |
| Hull 02 | 0.956 | 0.971 | 0.978 | 0.983 | 0.987 | 0.995 | 0.994 | 0.993 | 0.992 | 0.992 |
| Hull 03 | 0.996 | 0.996 | 0.997 | 0.998 | 0.998 | 0.997 | 0.996 | 0.996 | 0.995 | 0.996 |
| Hull 04 | 0.997 | 0.997 | 0.998 | 0.999 | 0.999 | 0.997 | 0.996 | 0.996 | 0.996 | 0.996 |
| Hull 05 | 0.998 | 0.997 | 0.998 | 0.998 | 0.998 | 0.997 | 0.996 | 0.996 | 0.996 | 0.997 |
| Hull 06 | 0.981 | 0.986 | 0.989 | 0.991 | 0.993 | 0.997 | 0.996 | 0.994 | 0.994 | 0.994 |
| Hull 07 | 0.999 | 0.999 | 0.999 | 0.999 | 0.999 | 0.999 | 0.999 | 0.998 | 0.998 | 0.999 |
| Hull 08 | 0.999 | 0.999 | 0.999 | 0.999 | 0.999 | 0.999 | 0.999 | 0.998 | 0.998 | 0.999 |
| Hull 09 | 0.984 | 0.987 | 0.990 | 0.992 | 0.994 | 0.999 | 0.998 | 0.997 | 0.997 | 0.997 |
| Hull 10 | 0.986 | 0.989 | 0.992 | 0.993 | 0.995 | 0.996 | 0.995 | 0.994 | 0.992 | 0.994 |
| Hull 11 | 0.998 | 0.997 | 0.998 | 0.998 | 0.999 | 0.999 | 0.998 | 0.998 | 0.997 | 0.998 |
| Hull 12 | 0.997 | 0.997 | 0.997 | 0.998 | 0.999 | 0.999 | 0.998 | 0.997 | 0.997 | 0.998 |
| Hull 13 | 0.999 | 0.998 | 0.998 | 0.998 | 0.999 | 0.999 | 0.998 | 0.997 | 0.997 | 0.998 |
| Hull 14 | 0.992 | 0.993 | 0.995 | 0.995 | 0.996 | 0.999 | 0.999 | 0.998 | 0.998 | 0.999 |
| Hull 15 | 0.999 | 0.999 | 0.999 | 0.998 | 1.000 | 1.000 | 0.999 | 0.999 | 0.998 | 0.999 |
| Hull 16 | 1.000 | 0.999 | 0.999 | 0.998 | 1.000 | 1.000 | 0.999 | 0.999 | 0.998 | 0.999 |
| Hull 17 | 0.992 | 0.993 | 0.994 | 0.995 | 0.997 | 0.999 | 0.998 | 0.997 | 0.996 | 0.997 |
| Hull 18 | 0.999 | 0.998 | 0.998 | 0.998 | 0.999 | 0.999 | 0.998 | 0.997 | 0.997 | 0.998 |
| Hull 19 | 0.996 | 0.997 | 0.997 | 0.997 | 0.999 | 0.999 | 0.999 | 0.998 | 0.997 | 0.999 |
| Hull 20 | 0.997 | 0.997 | 0.997 | 0.998 | 0.999 | 0.999 | 0.998 | 0.998 | 0.997 | 0.998 |
| Hull 21 | 0.996 | 0.997 | 0.997 | 0.997 | 0.998 | 1.000 | 0.999 | 0.998 | 0.998 | 0.999 |
| Hull 22 | 0.996 | 0.996 | 0.997 | 0.997 | 0.997 | 1.000 | 0.999 | 0.998 | 0.998 | 0.999 |
| Hull 23 | 0.997 | 0.997 | 0.997 | 0.998 | 0.999 | 0.999 | 0.998 | 0.997 | 0.996 | 0.997 |
| Hull 24 | 0.975 | 0.982 | 0.986 | 0.988 | 0.991 | 0.992 | 0.991 | 0.989 | 0.988 | 0.988 |
| Hull 25 | 0.993 | 0.994 | 0.995 | 0.996 | 0.998 | 0.999 | 0.998 | 0.997 | 0.996 | 0.998 |
| min | 0.956 | 0.971 | 0.978 | 0.983 | 0.987 | 0.992 | 0.991 | 0.989 | 0.988 | 0.988 |
| max | 1.000 | 0.999 | 0.999 | 0.999 | 1.000 | 1.000 | 0.999 | 0.999 | 0.998 | 0.999 |
| mean | 0.993 | 0.994 | 0.995 | 0.996 | 0.997 | 0.998 | 0.997 | 0.997 | 0.996 | 0.997 |

above 0.880 for each vessel and speed. Therefore, the significance of the proposed model for $Im(\zeta)$ is still good for the database reproduction.

Table 10 reports the quality of fit, expressed according to the metric of $R^2$, for the complex pitch transfer functions. Considering the real part $Re(\theta)$, the general level of fitting quality is extremely high, having average values for each speed always above 0.990. For the speed of 10.0 knots, the average $R^2$ value is 0.993, with a minimum of 0.956 for Hull 02. At $V_s = 12.5$ knots, the average $R^2$ increases to 0.994, with a minimum of 0.971 for Hull 02. Increasing $V_s$ to 15.0 knots, the average $R^2$ goes to 0.995, with a minimum of 0.978 always for Hull 02. For a speed of 17.5 knots, the average quality of fit is 0.996, with a minimum of 0.983 for Hull 02. Finally, the speed of 20.0 knots registers an aver-

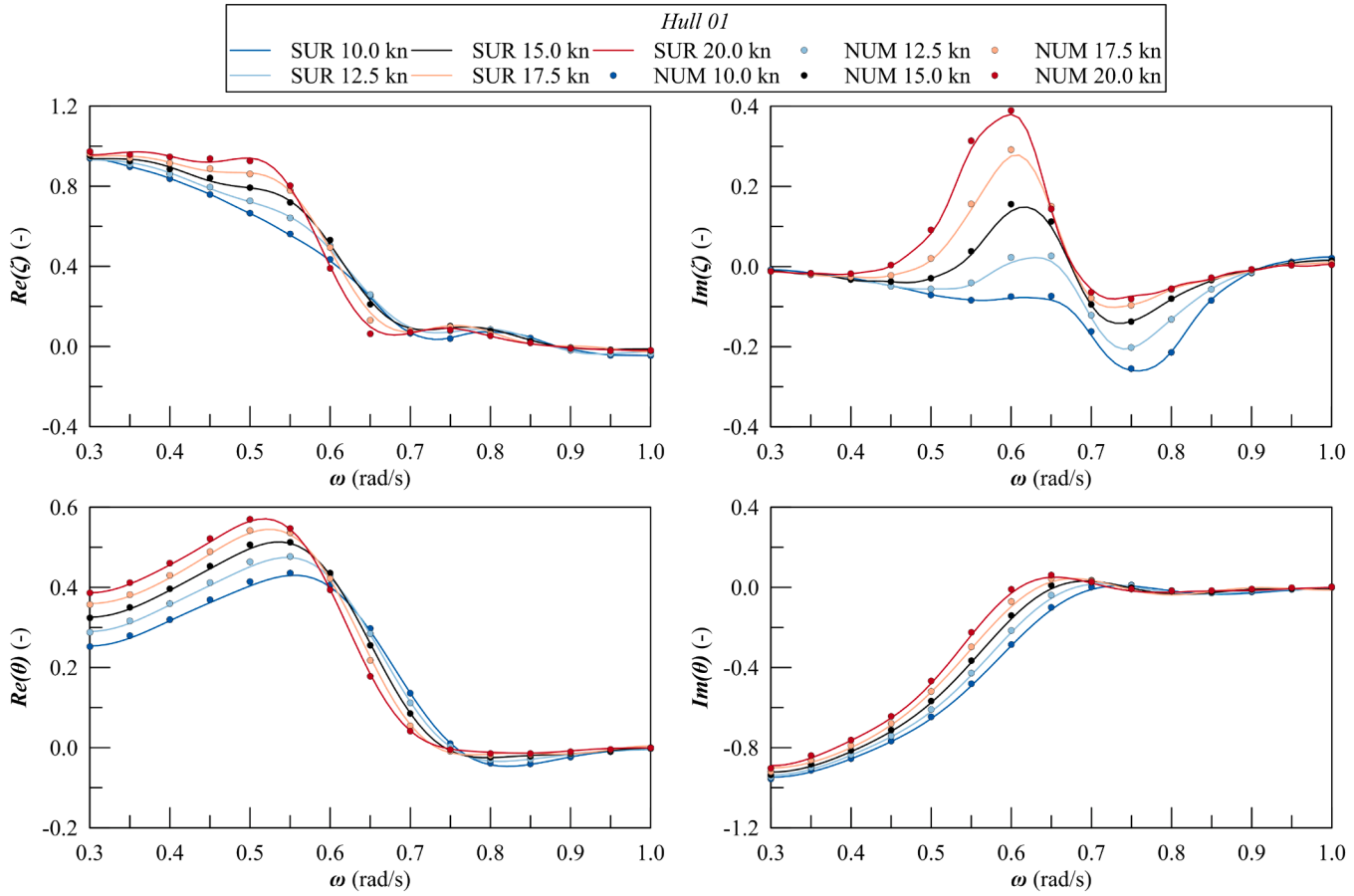


**Fig. 8.** Comparison between numerical (NUM) and surrogate (SUR) TRFs for hull 01.

age $R^2$ of 0.997, with a minimum of 0.987 for Hull 02. For the case of $Re(\theta)$, the minimum quality of fit is always registered for Hull 02, but still keeping a reasonably high $R^2$ value. Taking into consideration the quality of fit indicators of the individual harmonics $a_i$ (see Section 4), the moderate quality obtained for some of the $a_i$ is not reflecting in the global fitting of the real part of the complex transfer function for all the selected speed range. Therefore, the significance of the proposed model for $Re(\theta)$ is really good for the database reproduction.

At last, considering the imaginary part $Im(\theta)$ of the pitch transfer function, the values reported in Table 10 are also identifying good fitting performances. At a speed of 10.0 knots, the average $R^2$ value is 0.998, with a minimum of 0.992 for Hull 24. Increasing the speed to 12.5 knots, the average value of $R^2$ lowers to 0.997, with a minimum of 0.991 for Hull 24. For $V_s = 15.0$ knots, the average $R^2$ is 0.997, with a lower value for Hull 24 of 0.989. At a speed of 17.5 knots, the average $R^2$ is 0.996, with a minimum (always for Hull 24) of 0.988. Finally, for the speed of 20.0 knots, the average $R^2$ value is 0.997, with a minimum of 0.988 for Hull 24. Also in this case, the worst quality of fit is obtained for a single hull form (in this case Hull 24), but keeping in any case a relatively high $R^2$ value (always above 0.985). A good quality of fit for $Im(\theta)$ is obtained despite the moderate quality of fit obtained for some harmonics in the model. Therefore, it can be concluded that the proposed model for $Im(\theta)$ is really good for the database reproduction.

As an example, Fig. 8 shows the comparison between surrogate and numerical complex transfer functions for Hull 01. From the figure, the really good level of fitting achievable with the proposed model is immediately recognisable. Hull 01 is an example of a vessel that has high quality of fit values for all the transfer functions, therefore a good fitting quality is expectable. For a fair report, Fig. 9 shows the comparison between surrogate and numerical complex transfer function for Hull 02, a ship representing the worst fitting performance for $Re(\theta)$ at all speeds and for $Im(\zeta)$ at the speed of 15,0 and 17.5 knots. Thus representing a case were the fitting is not extremely good. Considering the figure, it is possible to observe that for the heave function, there is a bit of overestimation for both $Re(\zeta)$ and $Im(\zeta)$ in the range of frequency between 0.45 and 0.65 rad/s. For the pitch transfer functions, there is a overestimation between 0.3 and 0.6 rad/s for both real and imaginary part. In any case, taking into considerations all the mentioned issues, it is possible to observe that also in this case the global trend of the complex transfer function is captured.

It can be concluded that the proposed models for complex transfer functions for heave and pitch motions in head sea for the five calculation speed is representing really well the initial database. However, the present verification study considers only the reproduction of the transfer functions. Then, additional investigation is needed on the effect of using surrogate models in the estimation of ship comfort.

### 5.2. Comfort analysis on general cruise ships

After the verification of the proposed models for the surrogate complex transfer function, it is necessary to understand the applicability of the method to the estimation of comfort performances on a general cruise ship. To this end, it is proposed to apply the surrogate models to the estimation of the comfort rating $CR_V$ (described by Eq. (6)) on six cruise ships external to the initial database. Then, the comfort rating results will be compared with the ones resulting from the use of numerical transfer functions on the same ships.

The reference ships have the dimensions reported in Table 11, while Fig. 10 shows the transversal view of the vessel's body plans. All the parameters are inside the limits of the initial database; thus, the

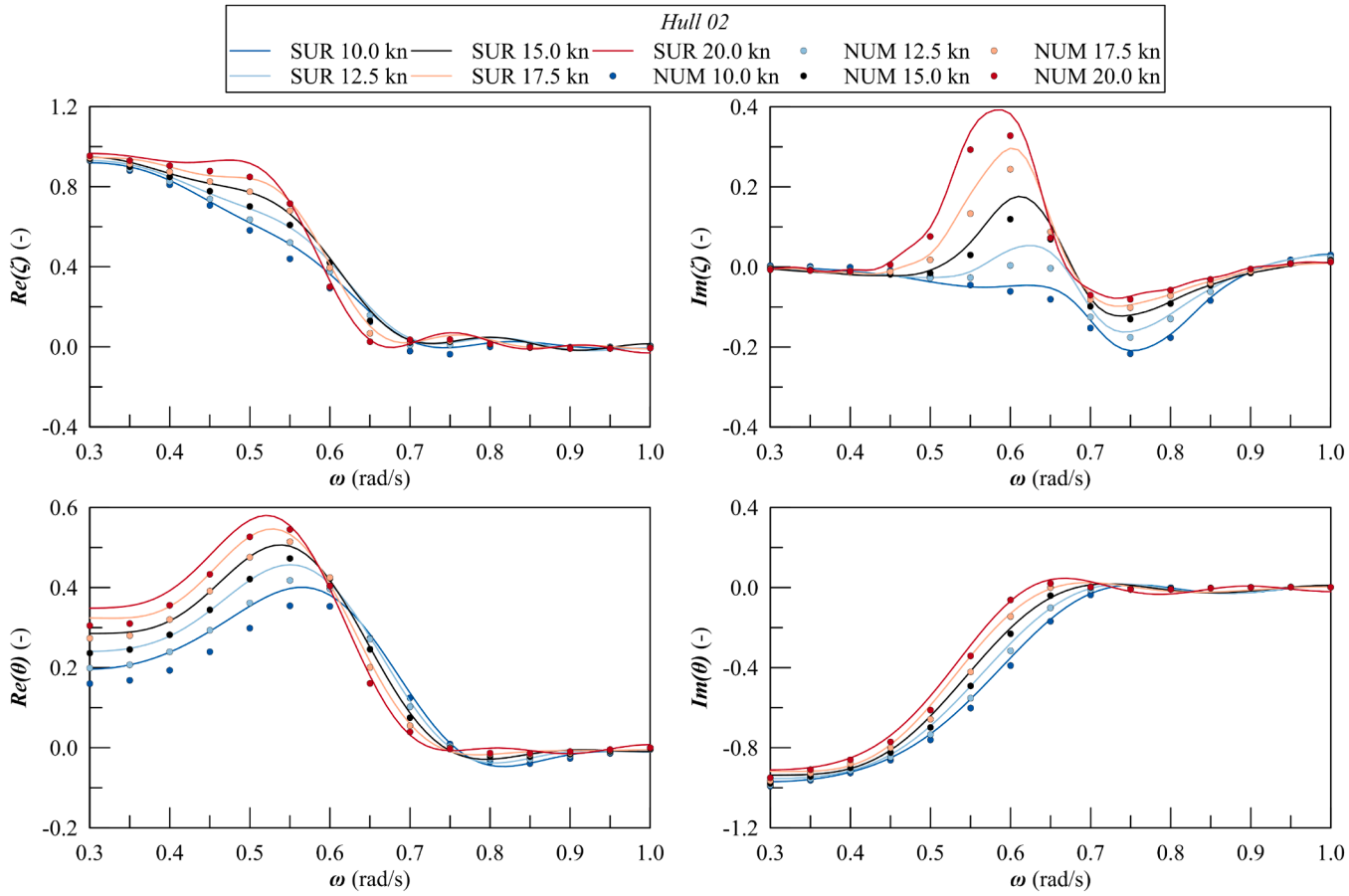


**Fig. 9.** Comparison between numerical (NUM) and surrogate (SUR) TRFs for hull 02.

**Table 11**
General particulars of the six reference cruise ships.

| | Symbol | REF_01 Value | REF_02 | REF_03 | REF_04 | REF_05 | REF_06 | Unit |
|---|---|---|---|---|---|---|---|---|
| Length between perpendiculars | $L_{PP}$ | 165.00 | 164.50 | 163.98 | 179.70 | 177.12 | 164.62 | m |
| Waterline length | $L_{WL}$ | 168.00 | 167.50 | 166.93 | 182.93 | 180.31 | 167.58 | m |
| Breadth | $B$ | 25.00 | 24.50 | 23.38 | 25.62 | 24.50 | 24.50 | m |
| Draught | $T$ | 6.00 | 6.00 | 6.00 | 6.00 | 6.00 | 6.00 | m |
| Volume | $\nabla$ | 17130.14 | 16997.41 | 16638.34 | 19978.91 | 18266.23 | 17875.44 | $m^3$ |
| Wetted surface | $S$ | 4911.04 | 4912.49 | 4647.39 | 5421.30 | 5104.78 | 4848.72 | $m^2$ |
| Longitudinal centre of buoyancy | $x_B$ | 83.62 | 76.57 | 83.62 | 91.63 | 90.05 | 83.39 | m |
| Vertical centre of buoyancy | $z_B$ | 3.36 | 3.35 | 3.35 | 3.35 | 3.36 | 3.32 | m |
| Block coefficient | $C_B$ | 0.663 | 0.673 | 0.694 | 0.694 | 0.673 | 0.709 | – |
| Prismatic coefficient | $C_P$ | 0.702 | 0.715 | 0.734 | 0.734 | .712 | 0.750 | – |
| Midship coefficient | $C_x$ | 0.945 | 0.940 | 0.945 | 0.945 | 0.945 | 0.945 | – |
| Length/Breadth ratio | $L/B$ | 6.720 | 6.837 | 7.140 | 7.140 | 7.360 | 6.840 | – |
| Breath/Draught ratio | $B/T$ | 4.167 | 4.083 | 3.897 | 4.270 | 4.083 | 4.083 | – |

proposed methodology should be applicable to the selected cruise ships. On the reference ships, 2D strip theory calculations have been carried out considering the same conditions employed for the database development, resulting in the availability of the numerical heave and pitch transfer functions for head seas at the speeds of 10.0, 12.5, 15.0, 17.5 and 20.0 knots.

As an example, Fig. 11 shows the comparison between the complex transfer functions obtained with the surrogate models and the computed ones for all the speeds in head sea for ship REF_01. It is possible to observe the same issues made for the representation of Hull 06 (Fig. 9). To have an idea of the quality of fit achieved for the reference hulls, the $R^2$ coefficient has been calculated also for these cases. Table 12 reports the $R^2$ obtained for all the five speed on the real and imaginary part of heave and pitch transfer functions. It can be observed that the quality of fit values are all above 0.9. The worst fitting performances are for $Im(\zeta)$; however, considering Fig. 11 for ship REF_01, the trend of the function is still captured. This trend has been observed for all the remaining reference hulls, but are not reported here for the sake of brevity. There is a difference between initial amplitude of the numerical and surrogate complex TRFs for all the cases. This is due to the fitting of the $a_0$ coefficient. Being the $R^2$ value not close to 1, there is a difference in the mean value of the real and surrogate complex TRFs. It should be checked whether this matter affects the evaluation of the $CR_V$ index.

Notwithstanding the above, a pure verification based on the fitting of the complex TRFs is not sufficient to judge the quality and applicability of the method for concept design purposes. Designers are interested in

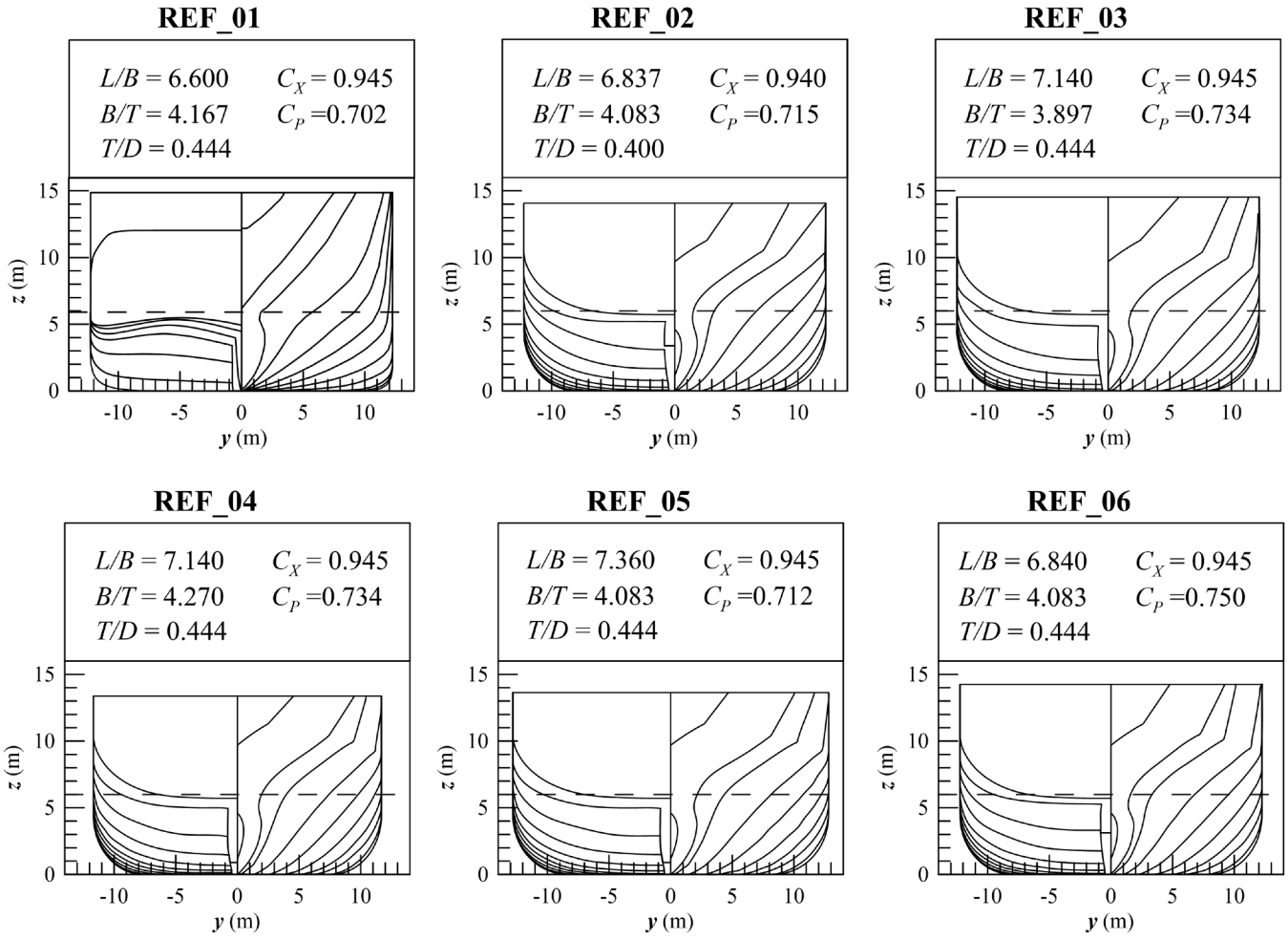


**Fig. 10.** Transversal body plan of the six reference ships.

ship attributes, like motion-induced comfort, which derives from the application of TRFs into an assessment framework. Therefore, the present model is here applied to the framework presented in Section 2.3, evaluating the comfort rating $CR_V$ as described in Section 2.2. In parallel, the same framework is applied to the numerical TRFs calculated for the reference cruise ships, allowing for a fair comparison between the comfort ratings evaluated with surrogate and numerical models.

As highlighted in Section 2.2, the evaluation of the $CR_V$ index is influenced by the selection of $H_s$ and $T_z$ couples for the motion analysis. The calculation couples changes according to the selected sea areas of interest and the discretisation level of the calculations. For the reference sea areas, as already mentioned, a combination between Area 26, 27 and 47 of the Global Wave Statistics is selected. For the discretisation, it has been decided to employ the continuous joint $H_s - T_z$ distributions for the selected areas (DNV, 2014) in order to reduce the effect of discretisation on the final results. Such an approach changes the methodology necessary to calculate $CR_V$ according to Eq. (6).

The joint probability distribution of $H_s$ and $T_z$ is given by:

$$f_{H_s,T_z}(h,t) = f_{H_s}(h) f_{T_z|H_s}(t|h) \tag{28}$$

The marginal distribution of $H_s$ is conveniently modeled with a 3 parameters Weibull distribution:

$$f_{H_s}(h) = \frac{\beta_H}{\alpha_H}\left(\frac{h-\gamma_H}{\alpha_H}\right)^{\beta_H-1} \exp -\left(\frac{h-\gamma_H}{\alpha_H}\right)^{\beta_H} \tag{29}$$

where $\alpha_H$, $\beta_H$ and $\gamma_H$ are the shape, scale and location parameters, respectively. The remaining function in Eq. (28) is the conditional distribution of $T_z$ with respect to $H_s$. This function is well represented by a log-normal distribution, providing the following formula:

$$f_{T_z|H_s}(t|h) = \frac{1}{\sigma t\sqrt{2\pi}} \exp -\frac{(\ln t - \mu)^2}{2\sigma^2} \tag{30}$$

where the parameters $\sigma$ and $\mu$ are expressed as a function of $h$ according to the following expressions:

$$\mu = a_0 + a_1 h^{a_2} \tag{31}$$

$$\sigma = b_0 + b_1 \exp\left(b_2 h\right) \tag{32}$$

the coefficients $a_i$, $b_i$ $(i = 0, 1, 2)$, $\alpha_H$, $\beta_H$ and $\gamma_H$ derive from the wave statistics of each sea area. Table 13 resumes the coefficients for the three selected sea areas.

Knowing the joint distributions, the effective evaluation of $CR_V$ may follow a nondeterministic multidimensional Monte Carlo (MC) integration process. The general approximation of a MC integral is as follows:

$$\int_\Omega f(\mathbf{x})\mathrm{d}\mathbf{x} \approx \frac{1}{N_s}\int_\Omega \mathrm{d}\mathbf{x} \sum_{i=1}^{N_s} f\left(x_i\right) \tag{33}$$

where $\Omega \subset \mathbb{R}^m$ is an $m$-dimensional probability space, $\mathbf{x} \in \Omega$ is a set of $m$ independent random variables and $N_s$ is the number of samples. For convenience, $\Omega$ is defined as an unit hypercube $(0,1)^m$ in order to have $\int_\Omega \mathrm{d}\mathbf{x} = 1$. Then, uniform random variables $\mathbf{U} \sim \mathbb{U}(0,1)$ define $\mathbf{x}$. According to these assumptions, Eq. (33) becomes:

$$\int_\Omega f(\mathbf{x})\mathrm{d}\mathbf{x} \approx \frac{1}{N_s} \sum_{i=1}^{N_s} f\left(\mathbf{U}_i\right) \tag{34}$$

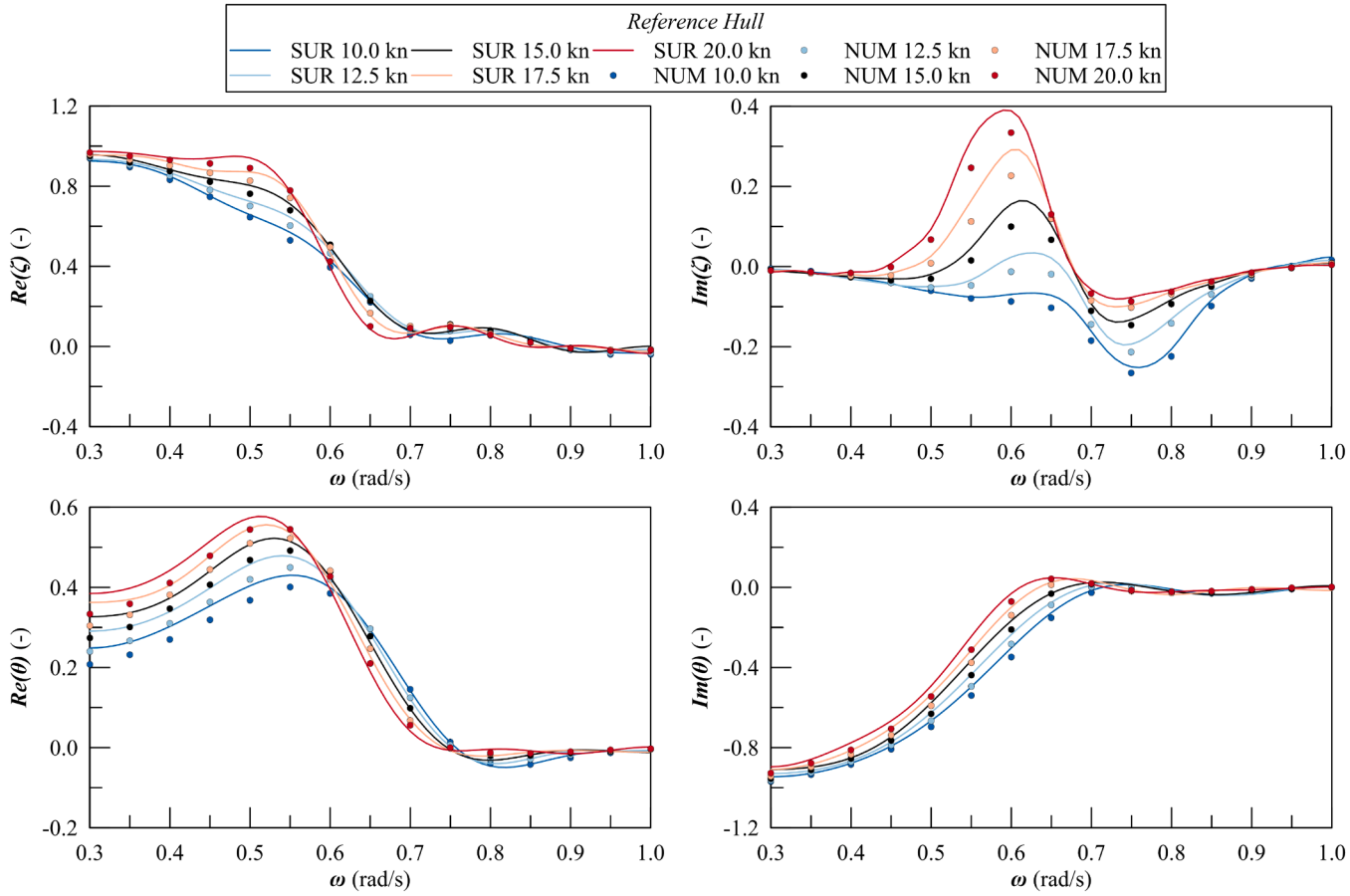


**Fig. 11.** Comparison between numerical (NUM) and surrogate (SUR) TRFs for the reference hull REF_01.

By employing the above described MC process, the calculation of $CR_V$ cannot be performed anymore with Eq. (6), but results from:

$$CR_V = \sum_{i=1}^{N_L} p_{L_i} \frac{1}{N_s} \sum_{j=1}^{N_s} f_{H_s,T_z}(\mathbf{U}) I_{CR_{ij}} \tag{35}$$

where $I_{CR}$ is always defined by Eq. (7). As the joint distribution $f_{H_s,T_z}$ is a function of the uniform random variables $\mathbf{U}$, the sampling process needed to generate $\mathbf{U}$ influences the results (Mauro and Vassalos, 2022). The conventional method for MC processes consists in performing a direct sampling of $\mathbf{U}$ with pseudo-random numbers, adopting a so-called *crude MC method* (Niederreiter, 1987). To facilitate the integral convergence and lower the $N_s$ necessary to achieve the integral solution, the present work employs a Quasi-MC process (QMC) (Mauro and Nabergoj, 2022), generating $\mathbf{U}$ by means of quasi-random numbers resulting from a Sobol sequence (Sobol et al., 2011). The resolution of a QMC integral is the same of a MC one, but it has the advantage of be reproducible and to converge with a lower amount of samples (Mauro and Nabergoj, 2024). In any case, the joint distribution $f_{H_s,T_z}$ is not uniform, therefore it should be derived from $\mathbf{U}$. This is performed through the inversion of the cumulative density function $F(x)$. Being $\mathbf{U}$ uniform in $[0,1]$, $F^{-1}(\mathbf{U})$ is distributed according to $F$, and, for a generic variable $X$, the cumulative $F(\mathbf{X})$ is consequently uniform in $[0,1]$. This property is valid also for multidimensional variables, thus apply to joint distributions.

Therefore, the QMC process for the calculation of $CR_V$ can be summarised in the following steps:

1. Generation of $\mathbf{U} = \left(u_{H_s}, u_{T_z}\right) \in [0,1]^2$ with a Sobol sequence.
2. Compute $F_{H_s}^{-1}(h)$ from the probability density function (PDF) of Eq. (29).
3. Compute $F_{T_z|H_s}^{-1}(h,t)$ from the PDF of Eq. (30).
4. Compute $H_s$ and $T_z$ as follows:

$$\begin{cases} H_s = F_{H_s}^{-1}\left(u_{H_s}\right) \\ T_z = F_{T_z}^{-1}\left(u_{T_z}|u_{H_s}\right) \end{cases} \tag{36}$$

5. Estimate $\ddot{\xi}$ and $MSI$ for the different locations.
6. Compute $CR_V$ according to Eq. (35)

As already mentioned in Section 2, the comfort analysis has to be performed on points of interest for the ship. Dealing only with head sea conditions, the motions are only influenced by the longitudinal position of the calculation points. Therefore, the four calculation points have the following $x$ coordinate:

- *Point#1*: at $x/L_{pp} = 0.03$, representing the swimming pool.
- *Point#2*: at $x/L_{pp} = 0.21$, representing the principal attraction.
- *Point#3*: at $x/L_{pp} = 0.67$, representing the most valuable cabins.
- *Point#4*: at $x/L_{pp} = 0.90$, representing the wheel house.

Having the absolute locations $x$ allows for determine the relative positions from the centre of gravity for all the reference ships (with $x_G$ located at the same longitudinal position of $x_B$), needed to determine the local motions and accelerations. All the distances are given from the aft perpendicular.

Calculations have been performed for the reference ships by employing both surrogate and numerical transfer functions. Fig. 12 shows the results of the QMC calculation process for both surrogate and numerical TRFs at the speed of 15.0 knots for the four locations. Thus, the graphs represent the calculation of an intermediate comfort coefficient $CR_{VL}$ which is location and speed specific. Here, for the sake of brevity, the

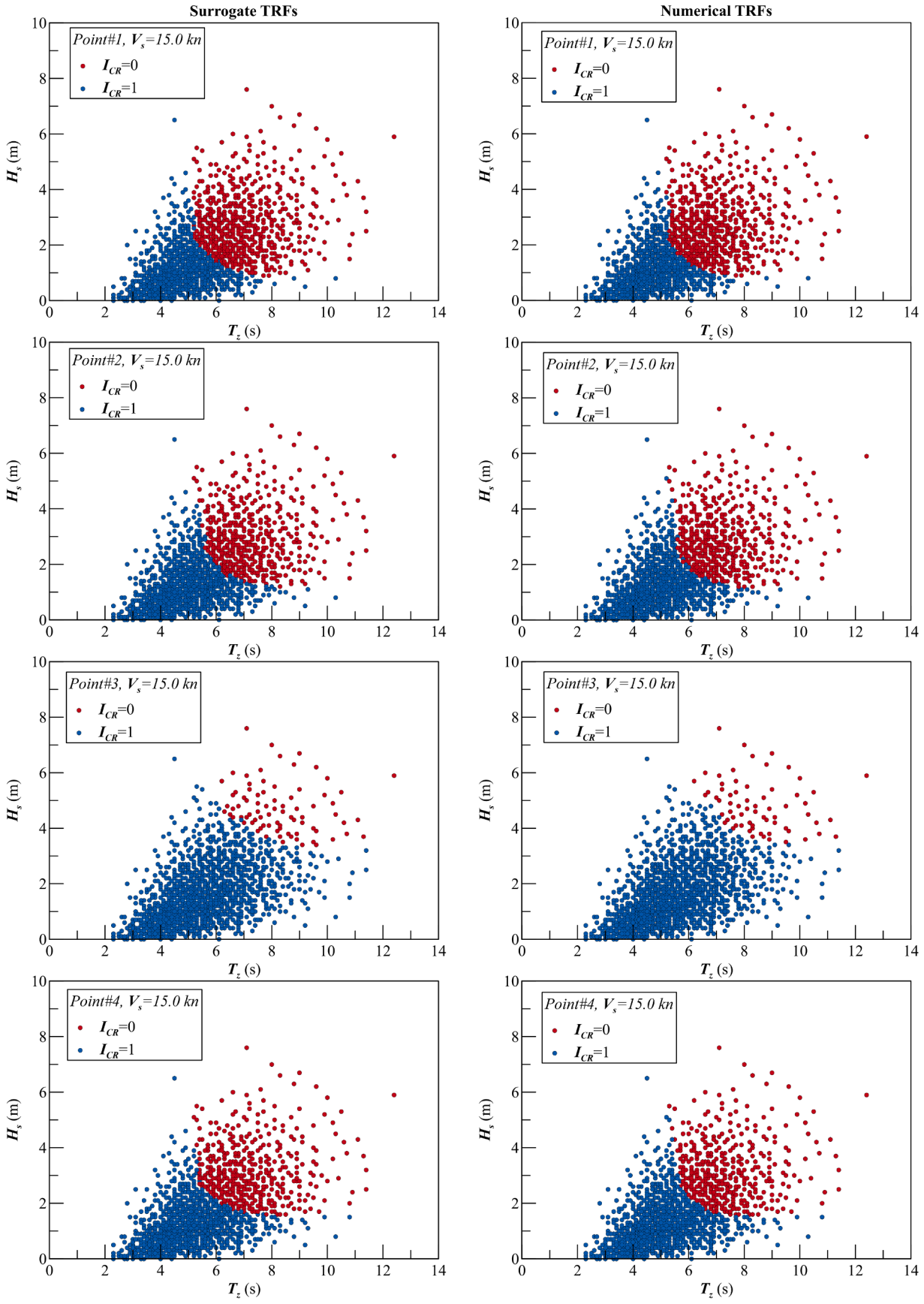


**Fig. 12.** $CR_{VL}$ evaluation at the speed of 15.0 knots with surrogate and numerical transfer functions for ship REF_01.

**Table 12**
Quality of fit for the complex transfer functions on the reference cruise ships.

| REF_01 | | | | |
|---|---|---|---|---|
| $V_s$ (kn) | $Re(\zeta)$ | $Im(\zeta)$ | $Re(\theta)$ | $Im(\theta)$ |
| 10.0 | 0.998 | 0.969 | 0.983 | 0.997 |
| 12.5 | 0.998 | 0.908 | 0.985 | 0.995 |
| 15.0 | 0.997 | 0.864 | 0.987 | 0.993 |
| 17.5 | 0.997 | 0.916 | 0.987 | 0.993 |
| 20.0 | 0.996 | 0.951 | 0.988 | 0.993 |
| REF_02 | | | | |
| $V_s$ (kn) | $Re(\zeta)$ | $Im(\zeta)$ | $Re(\theta)$ | $Im(\theta)$ |
| 10.0 | 0.995 | 0.961 | 0.981 | 0.991 |
| 12.5 | 0.995 | 0.904 | 0.983 | 0.994 |
| 15.0 | 0.991 | 0.861 | 0.981 | 0.992 |
| 17.5 | 0.994 | 0.913 | 0.981 | 0.992 |
| 20.0 | 0.991 | 0.953 | 0.985 | 0.990 |
| REF_03 | | | | |
| $V_s$ (kn) | $Re(\zeta)$ | $Im(\zeta)$ | $Re(\theta)$ | $Im(\theta)$ |
| 10.0 | 0.992 | 0.967 | 0.981 | 0.993 |
| 12.5 | 0.992 | 0.904 | 0.982 | 0.993 |
| 15.0 | 0.994 | 0.861 | 0.985 | 0.991 |
| 17.5 | 0.991 | 0.911 | 0.984 | 0.991 |
| 20.0 | 0.991 | 0.954 | 0.984 | 0.991 |
| REF_04 | | | | |
| $V_s$ (kn) | $Re(\zeta)$ | $Im(\zeta)$ | $Re(\theta)$ | $Im(\theta)$ |
| 10.0 | 0.994 | 0.961 | 0.981 | 0.996 |
| 12.5 | 0.994 | 0.902 | 0.981 | 0.991 |
| 15.0 | 0.992 | 0.860 | 0.983 | 0.991 |
| 17.5 | 0.993 | 0.912 | 0.984 | 0.992 |
| 20.0 | 0.993 | 0.948 | 0.989 | 0.994 |
| REF_05 | | | | |
| $V_s$ (kn) | $Re(\zeta)$ | $Im(\zeta)$ | $Re(\theta)$ | $Im(\theta)$ |
| 10.0 | 0.994 | 0.965 | 0.981 | 0.995 |
| 12.5 | 0.994 | 0.904 | 0.981 | 0.994 |
| 15.0 | 0.993 | 0.860 | 0.985 | 0.992 |
| 17.5 | 0.993 | 0.915 | 0.984 | 0.992 |
| 20.0 | 0.995 | 0.949 | 0.986 | 0.992 |
| REF_06 | | | | |
| $V_s$ (kn) | $Re(\zeta)$ | $Im(\zeta)$ | $Re(\theta)$ | $Im(\theta)$ |
| 10.0 | 0.995 | 0.954 | 0.981 | 0.993 |
| 12.5 | 0.995 | 0.899 | 0.981 | 0.992 |
| 15.0 | 0.994 | 0.861 | 0.984 | 0.990 |
| 17.5 | 0.994 | 0.913 | 0.984 | 0.991 |
| 20.0 | 0.995 | 0.947 | 0.983 | 0.991 |

only case of ship REF_01 is reported graphically. From the figure, it is extremely difficult to notice a difference between the surrogate and numerical results. However, to properly draw some conclusions it is more useful to consider the $CR_V$ and $CR_{VL}$ values.

Table 14 reports the obtained results for all the four speeds and locations (the $CR_{VL}$ indices), together with the comfort rating $CR_V$ for each specific speed on all the six reference ships. The evaluation of $CR_V$ has been performed assuming the weights $p_{L_i}$ equal. The $CR_V$ and $CR_{VL}$ values are reported in percentage form, indicating how long the ship can be considered comfortable in one year of service. Analysing the results, it is possible to observe that the differences in $CR_{VL}$ values is always under 1.5 %, with the worst agreement for *Point#2* at the speed of 20.0 knots for ship REF_01. Considering the $CR_V$, the global difference is always under 1.0 %. Also in this case, the worst agreement is for the speed of 20.0 knots and also in this case for ship REF_01.

A difference of 1.5 % implies an error of about 5 days an a half along the year of service, while the error of 1.0 % corresponds to less than 4 days. Such an error is more than acceptable during the concept design phase of a cruise ship, providing the possibility of predicting the comfort onboard with a level of accuracy comparable with an advanced stage of design, where hull form and direct numerical analysis are available.

## 6. Concluding remarks

The verification process presented in Section 5 shows that the provided model fits quite well the numerical TRFs of the initial database of 25 ships. Furthermore, the application of the methodology to six ships not included in the database highlights a good agreement between the comfort predictions obtained with numerical and surrogate TRFs. Such a results is of extremely high importance to the application of the method in the concept design stage, providing a surrogate model that is potentially accurate like a prediction performed with a numerical solver, usually available only in more advanced stages of the design.

Notwithstanding the above, the methodology can be further improved to be even more efficient and useful for concept design purposes. The following points can be further discussed and analysed:

- Regression methods for the surrogate models.
- Initial database dimensions.
- Encounter conditions and motions to include in the models.
- Source of the initial TRFs.

The following sections provide a point-by-point discussion on the above-mentioned topics.

### 6.1. Regression methodology

Even though the provided surrogate models have a good agreement with the initial TRFs of the starting database, some improvements can be further provided to the developed regressions. In fact, the reproduction of some of the harmonics $a_i$ by the surrogate models shows levels of quality of fit indicators that leads to models that are moderate significant for the considered $a_i$. This is the case, for example, of the intercept $a_0$ of $Re(\zeta)$, $Re(\theta)$ and $Im(\theta)$, where quality of fit indicators like $R^2$ are ranging between 0.65 and 0.75, thus representing a moderate significant correlation between the dependent and the independent variables. The not really good correlation for $a_0$, generates the shift noticed for several ships (like Hull 02 in Fig. 9) in the mean value of the complex TRFs.

Therefore, there is a margin of improvement for the provided models, trying to find a better correlation for some harmonics. A study in this direction has been already performed, increasing the order of the starting polynomial regression to 3 instead of 2. The resulting models highlight extremely good correlation levels for all the harmonics. However, the resulting global model fit really well only the initial database members, but drastically fail in the generalisation as values are oscillating to much between the points of the design space.

Such a matter is due to the structure of the database, as the CCF design suggests a model that is at most of the second order. In order to avoid this issue, it is necessary to increase the dimension of the initial database as it will be discussed in the coming section.

Finally, due to the relatively short amount of vessels that are currently composing the database, it is not advisable to abandon the multiple linear regression technique in favour of more advanced regression methods based on machine learning. Such a study is advisable only when a really wide and variegate database of TRFs is available.

### 6.2. Initial ships database

As mentioned above, a relevant improvement to the provided models can be achieved by increasing or changing the initial database of ships. The current database has been generated starting from a mother hull, modified according to the parameters variations described in Section 3. As such, the current database covers variations only for the $C_x$, $C_P$, $L/B$ and $B/T$, and, consequently, the surrogate models are only functions of these parameters.

**Table 13**
Coefficients for the joint $H_s - T_z$ distributions in the reference sea areas.

| Area | $\alpha_H$ | $\beta_H$ | $\gamma_H$ | $a_0$ | $a_1$ | $a_2$ | $b_0$ | $b_1$ | $b_2$ |
|---|---|---|---|---|---|---|---|---|---|
| Area 26 | 1.8100 | 1.3000 | 0.0000 | 0.7000 | 0.8580 | 0.2320 | 0.0700 | 0.1955 | -0.0497 |
| Area 27 | 1.7600 | 1.3000 | 0.0000 | 0.7000 | 0.8800 | 0.2180 | 0.0700 | 0.1879 | -0.0419 |
| Area 47 | 2.3000 | 1.7800 | 0.0000 | 0.7000 | 1.0580 | 0.1490 | 0.0700 | 0.1301 | -0.0250 |

**Table 14**
$CR_V$ and $CR_{VL}$ percentage values for the six reference ships according to numerical (NUM) and surrogate (SUR) TRFs.

| | REF_01 | | | | | | | | | |
|---|---|---|---|---|---|---|---|---|---|---|
| | $V_s$ = 10.0 kn | | $V_s$ = 12.5 kn | | $V_s$ = 15.0 kn | | $V_s$ = 17.5 kn | | $V_s$ = 20.0 kn | |
| | SUR | NUM | SUR | NUM | SUR | NUM | SUR | NUM | SUR | NUM |
| *Point#1* | 59.76 | 59.04 | 58.38 | 58.16 | 57.88 | 57.84 | 57.72 | 57.78 | 59.00 | 57.60 |
| *Point#2* | 70.40 | 69.60 | 68.52 | 67.94 | 67.58 | 66.96 | 67.32 | 66.30 | 67.24 | 65.72 |
| *Point#3* | 96.14 | 96.00 | 95.88 | 96.24 | 94.58 | 95.42 | 92.84 | 93.76 | 90.46 | 90.54 |
| *Point#4* | 70.74 | 71.48 | 70.54 | 72.06 | 70.18 | 72.16 | 71.66 | 72.62 | 72.76 | 71.52 |
| *Total* | 74.26 | 74.03 | 73.33 | 73.60 | 72.56 | 73.10 | 72.39 | 72.62 | 72.37 | 71.35 |
| | REF_02 | | | | | | | | | |
| | $V_s$ = 10.0 kn | | $V_s$ = 12.5 kn | | $V_s$ = 15.0 kn | | $V_s$ = 17.5 kn | | $V_s$ = 20.0 kn | |
| | SUR | NUM | SUR | NUM | SUR | NUM | SUR | NUM | SUR | NUM |
| *Point#1* | 59.50 | 58.56 | 58.20 | 57.76 | 58.01 | 57.74 | 57.95 | 57.60 | 57.66 | 57.22 |
| *Point#2* | 69.62 | 68.78 | 68.58 | 67.36 | 67.64 | 66.72 | 67.18 | 66.02 | 66.56 | 65.28 |
| *Point#3* | 95.16 | 96.14 | 95.40 | 96.14 | 95.12 | 95.74 | 92.18 | 93.88 | 89.96 | 90.08 |
| *Point#4* | 72.00 | 72.16 | 72.22 | 72.66 | 73.20 | 74.08 | 73.35 | 74.12 | 71.20 | 71.26 |
| *Total* | 74.07 | 73.91 | 73.60 | 73.48 | 73.49 | 73.57 | 72.67 | 72.91 | 71.35 | 70.96 |
| | REF_03 | | | | | | | | | |
| | $V_s$ = 10.0 kn | | $V_s$ = 12.5 kn | | $V_s$ = 15.0 kn | | $V_s$ = 17.5 kn | | $V_s$ = 20.0 kn | |
| | SUR | NUM | SUR | NUM | SUR | NUM | SUR | NUM | SUR | NUM |
| *Point#1* | 59.12 | 59.98 | 58.25 | 59.14 | 57.68 | 58.16 | 57.01 | 57.86 | 57.32 | 58.22 |
| *Point#2* | 70.28 | 70.82 | 68.00 | 68.90 | 66.74 | 67.52 | 65.60 | 66.68 | 67.30 | 66.56 |
| *Point#3* | 95.60 | 95.70 | 95.88 | 96.08 | 94.16 | 95.18 | 92.72 | 93.72 | 90.88 | 91.40 |
| *Point#4* | 70.48 | 71.52 | 71.25 | 72.12 | 70.38 | 71.36 | 70.32 | 71.30 | 70.81 | 71.76 |
| | REF_04 | | | | | | | | | |
| | $V_s$ = 10.0 kn | | $V_s$ = 12.5 kn | | $V_s$ = 15.0 kn | | $V_s$ = 17.5 kn | | $V_s$ = 20.0 kn | |
| | SUR | NUM | SUR | NUM | SUR | NUM | SUR | NUM | SUR | NUM |
| *Point#1* | 58.96 | 58.48 | 57.10 | 57.98 | 56.18 | 57.34 | 56.30 | 57.08 | 58.10 | 56.72 |
| *Point#2* | 69.86 | 69.58 | 68.18 | 67.98 | 66.94 | 66.72 | 66.32 | 65.90 | 65.45 | 65.06 |
| *Point#3* | 95.52 | 94.90 | 95.62 | 94.98 | 94.82 | 95.68 | 94.04 | 94.78 | 92.28 | 92.60 |
| *Point#4* | 69.52 | 70.30 | 69.14 | 70.28 | 68.26 | 72.18 | 69.84 | 73.04 | 69.50 | 72.48 |
| *Total* | 73.47 | 73.32 | 72.51 | 72.81 | 71.55 | 72.98 | 71.63 | 72.70 | 71.33 | 71.72 |
| | REF_05 | | | | | | | | | |
| | $V_s$ = 10.0 kn | | $V_s$ = 12.5 kn | | $V_s$ = 15.0 kn | | $V_s$ = 17.5 kn | | $V_s$ = 20.0 kn | |
| | SUR | NUM | SUR | NUM | SUR | NUM | SUR | NUM | SUR | NUM |
| *Point#1* | 55.56 | 54.46 | 54.91 | 53.90 | 54.74 | 54.44 | 53.22 | 54.28 | 52.95 | 53.80 |
| *Point#2* | 66.50 | 65.24 | 64.20 | 63.62 | 64.00 | 63.42 | 63.00 | 62.78 | 62.84 | 61.52 |
| *Point#3* | 94.52 | 93.66 | 95.52 | 93.80 | 93.50 | 94.64 | 92.86 | 93.66 | 90.58 | 91.42 |
| *Point#4* | 65.04 | 65.54 | 65.10 | 65.60 | 68.80 | 69.92 | 69.95 | 70.84 | 68.50 | 68.00 |
| *Total* | 70.41 | 69.73 | 69.93 | 69.23 | 70.26 | 70.61 | 69.76 | 70.39 | 68.72 | 68.69 |
| | REF_06 | | | | | | | | | |
| | $V_s$ = 10.0 kn | | $V_s$ = 12.5 kn | | $V_s$ = 15.0 kn | | $V_s$ = 17.5 kn | | $V_s$ = 20.0 kn | |
| | SUR | NUM | SUR | NUM | SUR | NUM | SUR | NUM | SUR | NUM |
| *Point#1* | 61.14 | 62.18 | 60.16 | 61.12 | 59.82 | 60.68 | 59.78 | 60.44 | 59.75 | 60.30 |
| *Point#2* | 71.74 | 73.44 | 69.80 | 71.62 | 69.45 | 70.54 | 68.94 | 69.64 | 68.46 | 69.02 |
| *Point#3* | 96.50 | 95.56 | 97.12 | 96.04 | 96.85 | 95.98 | 95.40 | 94.76 | 93.20 | 92.22 |
| *Point#4* | 72.16 | 71.78 | 71.90 | 72.36 | 72.14 | 72.86 | 72.00 | 72.68 | 71.80 | 71.40 |
| *Total* | 75.39 | 75.74 | 74.75 | 75.29 | 74.57 | 75.02 | 74.03 | 74.38 | 73.30 | 73.24 |

Previous studies in the field of motions predictions in the early stages of design highlighted a dependence from also other hull parameters such as the waterplane area coefficient $C_{WP}$ or the position of the center of floating $x_F$. Therefore, the hull form variations can be extended to include also additional variables. Furthermore, the database could be extended including more steps of variations for the parameters, allowing for increasing the order of the polynomial model for MLR analysis.

An additional step to the effective generalisation of the model would be the availability of a database of real ships, not created through DOE techniques. However, there is no open hull database in the literaturethat

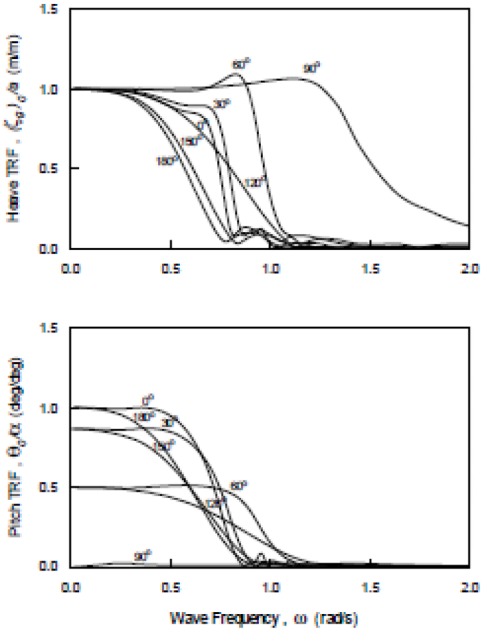


**Fig. 13.** Heave and pitch transfer functions at different headings for a vessel of 165 m length (Nabergoj, 2007).

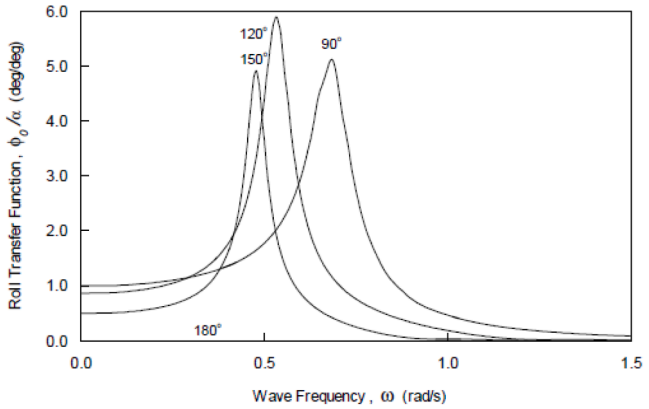


**Fig. 14.** Roll transfer functions at different headings for a vessel of 165 m length (Nabergoj, 2007).

may allow this option.

### 6.3. Encounter conditions and motions

The present study focuses on vertical motions for head sea conditions. This is for sure a limitation for an effective comfort assessment onboard a cruise ship, as also lateral motion for different encounter conditions are relevant to the effective estimation of comfort (see the discussion in Section 2). However, it has been decided to test the novel procedure based on the Fourier polynomial approximation on a single condition, where the reliability of the numerical instrument employed for TRFs evaluation is significantly high.

Notwithstanding the above, the proposed method shows a good potential in the reproduction of complex TRFs and it is reasonable to suppose that it could be accurate also for the prediction of motions for other encounter conditions, including the prediction of lateral motions. Further research will be carried out in the direction of extend the models to lateral motions for other encounter angles, enabling the consideration of other metrics for comfort (like the $EGA$), which requires estimations of lateral accelerations.

The TRFs for vertical motions does not change that much the global shape of the curve by changing the encounter angle. Fig. 13 shows an example of the heave and pitch transfer functions at different heading angles for a vessel having a length comparable with the ships employed for this study. From the figure it is evident that the oscillatory nature of the function does not change with the heading; therefore, the fitting process developed in this study can be applied without additional issues.

Another issue is the inclusion of lateral motions (i.e. the roll motion). In this case, the TRFs present an evident peak around the resonance frequency (see Fig. 14). In this case, additional effort should be taken to capture the position of the peak, probably requiring some modifications to the proposed regression model.

The inclusion of lateral motions in the prediction model, thus considering prediction of roll, will open some issues related to the calculation methods employed for the estimation of the initial TRFs, as it is discussed in the coming section.

### 6.4. Initial TRFs calculations

The global reliability of the prediction model is strongly dependent on the method employed for the calculation of initial TRFs. The TRFs employed in this work are coming from 2D strip theory calculations. The calculation method is coming from a state-of-the-art software and inherits all the limitations of the physics assumption on the base of the theory. This is not an issue for the motions considered in the study, as the method well capture the behaviour of vertical motions in head sea at different speeds. Such a matter has been widely discussed, validated and demonstrated in the literature. In any case, one of the main limitation of the methodology is the modelling of high sea states, where the 2D strip theory is not capable of capturing non-linearity associated with these particular sea states.

However, the employment of the same calculation techniques for lateral motions at different headings can be affected by the limitation of the method. Therefore, when approaching other environmental conditions, the nature of the calculation method has to be considered with care. It could be the case to select the employment of a 3D diffraction code, opportunely validated for different encounter headings and speeds, thus increasing the reliability of the obtained TRFs.

Particular focus should be dedicated to the prediction of roll motion. For the roll, the damping plays a delicate role, leading to the possible over-under estimation of the peak amplitude of the TRFs. Therefore, once approaching roll estimation, the validation of the model employed for damping on the mother hull of the database is essential to ensure surrogate model reliability.

Another thing to consider is that the present work does not include the possible presence of active devices for motion reduction, i.e. fins stabilisers. In case this should be considered in the analysis, dedicated calculations have to be carried out to derive the TRFs including the fins effect.

## 7. Conclusions

The work presented a novel methodology for the prediction of comfort onboard cruise ship in the concept design stage. Starting from an initial database of 25 ships, generated by means of design of experiment techniques, 2D strip theory calculations have been performed for five reference speed, obtaining the TRFs of heave and pitch motions in head seas. A surrogate model has been derived for these TRFs, fitting the real and imaginary part of the TRFs trough a Fourier polynomial, providing multiple linear regressions for the most relevant harmonics as a function of the vessels' main parameters. The obtained regressions have values for quality of fit indicators more than satisfactory, ensuing a good reproduction of the complex TRFs for all the 43 vessels of the database. To test the model generalisation inside the database bounds, surrogate transfer functions have been derived for six reference ships not included in the initial database, comparing the complex TRFs with the ones obtained

by means of numerical calculations. Also for this case, the comparison between numerical and surrogate TRFs shows a good agreement, confirming the quality of the proposed model. Furthermore, to verify the utility of the model for concept design purposes, the comfort rating $CR$ has been calculated on the reference ships for different locations and speeds employing the surrogate and numerical transfer functions. The results shows differences of maximum 1.5 % for the local $CR$ and 1.0 % for the global $CR$ at different speeds. Such difference correspond to less than 4.5 days in a year of operations. Therefore, the prediction accuracy of the model is comparable with the one resulting from direct numerical evaluation of TRFs. Such a result implies the suitability of the model for the comfort prediction of cruise ships in the concept design stage.

It has to be noticed that the current model is covering only vertical motions for head seas. Prediction of vertical and lateral motions for different vessel headings is also of interest in the prediction of comfort onboard, something that has not be considered in the present paper. However, being the intention of the paper to explore the development and applicability of a surrogate model considering both amplitude and phase of the TRFs, the work provides a solid basis for the extension of the regression model to other motions and encounter conditions. In fact, the extension of the procedure to different headings for heave and pitch motions does not represent a problem, being the shape of the TRFs similar. Different is the case of roll motion. In this case, fitting of the roll transfer function may require the necessity to reproduce the resonance peak of the TRF, probably introducing some differences in the proposed fitting process. However, such a matter should be carefully analysed in a dedicated research.

The reliability of the method can be further improved by changing the source of the initial TRFs database. The current model is based on 2D strip theory calculations, with all the limitations inherited by the calculation methodology. Even though a strip theory could be considered suitable for the prediction of vertical motions in head seas, this could be not the case for other encounter conditions and motions. However, the proposed methodology is independent from the source of the TRFs; therefore, it could be easily applied to TRFs coming from more advanced diffraction calculations or from experiments (if available).

In conclusion, the regression methodology developed and presented in this work provides a solid base for the further development of surrogate prediction models for the comfort onboard cruise ships, to be applied in the concept design stage. The method can be extended to other motions and encounter conditions, employing wider databases of calculations (including also different kinds of vessels), independently from the source of the TRFs. The work is the starting point for future studies and applications in the field of comfort and motions predictions in the concept design stage.

## CRediT authorship contribution statement

**F. Mauro:** Writing – review & editing, Writing – original draft, Supervision, Software, Methodology, Investigation, Formal analysis, Data curation, Conceptualization; **S. Utzeri:** Writing – review & editing, Software, Investigation, Data curation, Conceptualization; **J. Prpić-Oršić:** Writing – review & editing, Data curation; **L. Braidotti:** Writing – review & editing, Data curation, Conceptualization; **S. Bertagna:** Writing – review & editing; **V. Bucci:** Writing – review & editing.

## Declaration of competing interest

The authors declare that they have no known competing financial interests or personal relationships that could have appeared to influence the work reported in this paper.

## Acknowledgement

This work was supported by the Croatian Science Foundation under the project HRZZ-IP-2022-10-2821.

## Supplementary material

Supplementary material associated with this article can be found in the online version at 10.1016/j.oceaneng.2025.122825

## References

Andrews, D.J., 1998. A comprehensive methodology for the design of ships (and other complex systems). Proc. Math. Phys. Eng. Sci. 454, 187–211.
Andric, J., Prebeg, P., Palaversa, M., Zanic, V., 2021. Influence of topological variants on optimised structural scantlings of passenger ships. Mar. struct. 78, 102981.
Barone, G., Buonomano, A., Forzano, C., Palombo, A., 2021. Implementing the dynamic simulation approach for the design and optimization of ships energy systems: methodology and applicability to modern cruise ships. Renewable Sustainable Energy Rev. 150, 111488.
Begovic, E., Valentina, E.D., Mauro, F., Nabergoj, R., Rinauro, B., 2023. The impact of different bow shapes on large yacht comfort. J. Mar. Sci. Eng. 11(3), 495.
Box, G.E.P., Hunter, J.S., Hunter, W.J., 2005. Statistics for Experimenters. Design, Innovation and Discovery. Wiley.
Bucci, V., Sulligoi, G., Chalfant, J., Chryssostomidis, C., 2021. Evolution in design methodology for complex electric ships. J. Ship Prod. and Des. 37, 1–13.
Caprace, J.D., Rigo, P., 2011. Ship complexity assessment at the concept design stage. J. Mar. Sci. Technol. 16, 68–75.
DiGregorio, I., 2020. Development of a Stability Meta-Model for the Concept Design of Small Cruise Ships: Application of the IMO Second Generation Intact Stability Criteria. Master's thesis. University of Trieste.
DNV, 2014. DNV-RP-C205 Environmental Conditions and Environmental Loads. Technical Report. Det Norske Veritas.
Griffin, M.J., Whitham, E.M., 1980. Time dependency of whole-body vibration discomfort. JASA 68(5), 1522–1523.
Grin, R., 2024. On empirical methods to predict the rolling period of ships. In: Proceedings of 15th International Marine Design Conference (IMDC-2024), Amsterdam, The Netherlands.
Grin, R., van Heerd, J., Ferrari, V., 2013. Hydrodynamic aspects in the design of passenger vessels. In: Proceedings of RINA, Royal Institution of Naval Architects - Design and Operation of Passenger Ships.
Grin, R., Ruano, S.F., Bradbeer, N., Koelman, H., 2016. On the prediction of radii of inertia and their effect on seakeeping. In: Proceedings of PRADS 2016, Copenhagen, Denmark.
Grubišić, I., Žanić, V., Trincas, G., 1997. Sensitivity of multiattribute design to economic environment: shortsea Ro-Ro vessels. In: Proceedings of the 6th International Marine Design Conference, IMDC 97, pp. 201–216.
Hasselmann, K., Olbers, D., 1973. Measurements of wind-wave growth and swell decay during the joint North Sea wave project (JONSWAP). Ergänzung zur Deut. Hydrogr. Z. Reihe A 8(12), 1–95.
Hogben, N., Dacunha, N., Olliver, G., 1986. Global wave statistics. British Maritime Technology Limited.
Holtrop, J., 1984. Statistical re-analysis of resistance and propulsion data. Int. Shipbuild. Prog. 31(363), 272–276.
ISO, 1997. ISO 2631-1:1997 Mechanical vibration and shock - evaluation of human exposure to whole-body vibration. Technical Report. International Standard Organisation.
ISO, 2022. ISO 22834:2022 Large yachts - quality assessment of life onboard - stabilization and sea keeping. Technical Report. International Standard Organisation.
Jiang, P., Zhou, Q., Shao, X., 2020. Surrogate Model-Based Engineering Design and Optimization. Springer.
Kapsenberg, G.K., Aalbers, A.B., Koops, A., Block, J.J., 2015. Fast displacement ships, the MARIN systematic series. Technical Report. The Maritime Research Institute of the Netherlands, MARIN.
Liu, S., Papanikolaou, A., 2016. Fast approach to the estimation of the added resistance of ships in head waves. Ocean Eng. 112, 211–225.
Liu, S., Papanikolaou, A., 2020. Regression analysis of experimental data for added resistance in waves of arbitrary heading and development of a semi-empirical formula. Ocean Eng. 206, 107357.
Mauro, F., Benci, A., Ferrari, V., Valentina, E.D., 2021. Dynamic positioning analysis and comfort assessment for the early design stage of large yachts. Int. Shipbuild. Prog. 68(1–2), 33–60.
Mauro, F., Braidotti, L., Trincas, G., 2019a. Determination of an optimal fleet for a CNG transportation scenario in the mediterranean sea. Brodogradnja 70, 1–23.
Mauro, F., Braidotti, L., Trincas, G., 2019b. A model for intact and damaged stability evaluation of CNG ships during the concept design stage. J. Mar. Sci. Eng. 7, 450–473.
Mauro, F., Dell'Acqua, A., 2018. Vertical motions assessment of an offshore supply vessel in concept design stage. In: Technology and Science for the Ships of the Future - Proceedings of NAV 2018: 19th International Conference on Ship and Maritime Research, Trieste, Italy, pp. 380–387.
Mauro, F., Nabergoj, R., 2022. A probabilistic approach for dynamic positioning capability and operability predictions. Ocean Eng. 262, 112250.
Mauro, F., Nabergoj, R., 2024. Probabilistic evaluation of dynamic positioning operability with a quasi-Monte Carlo approach. Brodogradnja 75(1), 75105.
Mauro, F., Rosano, G., Begovic, E., Valentina, E.D., dell'Acqua, A., Rinauro, B., Tonelli, R., 2025. Towards a comprehensive hydrodynamic model for the feasibility study of motor yachts. J. Mar. Sci. Eng. 13(7), 1319.
Mauro, F., Valentina, E.D., Ferrari, V., Begovic, E., 2023. A method for early-stage design current loads determination on drill-ships. Ocean Eng. 287, 115716.
Mauro, F., Vassalos, D., 2022. The influence of damage breach sampling process on the direct assessment of ship survivability. Ocean Eng. 250, 111008.

Mauro, F., Vassalos, D., 2024a. The importance of first-principles tools in estimating passenger ship safety. Ocean Eng. 305, 117949.
Mauro, F., Vassalos, D., 2024b. Time to capsize for damaged passenger ships in adverse weather conditions. a multi-modal analysis. Ocean Eng. 299, 117409.
Nabergoj, R., 2007. Fondamenti di tenuta della nave al mare, University of Trieste, in italian.
Nabergoj, R., 2011. Station-keeping and seakeeping in offshore vessel design. In: Proceedings of 1st INT-NAM 2011, Istanbul, Turkey.
Niederreiter, H., 1987. Point sets and sequences with small discrepancy. Monatshefte für Mathematik 101(4), 273–337.
NORDFORSK, 1987. Assessment of Ship Performance in a Seaway. Technical Report. NORDFORSK.
Papanikolaou, A., 2014. Ship Design: Methodology of Preliminary Design. Springer.
Papanikolaou, A., 2019. A Holistic Approach to Ship Design. Springer.
Papanikolaou, A., Harries, S., Hooijmans, P., Marzi, J., Nena, R.L., Torben, S., Yrjan, A., Boden, B., 2022. A holistic approach to ship design: tools and applications. J. Ship Res. 66(1), 25–53.
Park, G.H., Hong, S., Percy, S., Kim, S.W., 2025. Techno-economic feasibility study of imported green hydrogen via inter-continental route: from Australia to South Korea. Appl. Energy 397, 126288.
Pintilie, A., Manea, M., Marasescu, D., Cristea, O., Burlacu, P., Clinci, C., Popa, N., 2025. Optimization of bulk carrier hull design through CAD modelling and FEM structural analysis - a case study. Results Eng. 26, 104846.
Radojčić, D., Kalajdžić, M., Zgradić, A.B., Simić, A., 2017. Resistance and trim modeling of a systematic planing hull series 62 (with 12.5 degrees, 25 degrees, and 30 degrees deadrise angles) using artificial neural networks, Part 2: mathematical models. J. Ship Prod. Des. 33(4), 257–275.
Rinauro, B., Begovic, E., Mauro, F., Rosano, G., 2024. Regression analysis for container ships in the early design stage. Ocean Eng. 292, 116499.
Rodrigues, M.I., Iemma, A.F., 2014. Experimental Design and Process Optimization. Taylor & Francis.
Salvesen, N., Tuck, E.O., Faltinsen, O., 1970. Ship motions and sea loads. Trans. Soc. Nav. Arch. Marine Eng. 78, 250–287.
Sayli, A., Alkan, A.D., Nabergoj, R., Uysal, A.O., 2007. Seakeeping assessment of fishing vessels in conceptual design stage. Ocean Eng. 34(5–6), 724–738.
Seo, S., Park, S., Koo, B., 2017. Effect of wave periods on added resistance and motions of a ship in head sea simulations. Ocean Eng. 137, 309–327.
Sobol, I., Asotky, D., Krenin, A., Kucherenko, S., 2011. Construction and comparison of high-dimensional sobol generations. Wilmott J. 64–73.
Trincas, G., 1989. An effective decision-making model for optimizing propulsive performance of fishing vessels in a seaway. In: Proceedings of the Internationales Rostocker Schiffstechnisches Symposium, Rostok, pp. 244–267.
Trincas, G., 2001. Survey of design methods and illustration of multiattributes decision making system for concept ship design. In: Proceedings of MARIND 2001, Varna, Bulgaria.
Vassalos, D., Paterson, D., Mauro, F., Mujeeb-Ahmed, M.P., Boulougouris, E., 2022. Process, methods and tools for ship damage stability and flooding risk assessment. Ocean Eng. 266, 113062.
Wang, C., Liu, X., Zhou, Y., Qian, J., 2025. Optimization of speed and refueling strategy for liner shipping companies considering refueling at OPL. Reg. Stud. Mar. Sci. 89, 104355.
Weisberg, S., 2005. Applied Linear Regression: Third Edition. Wiley Blackwell.
Žanić, V., 2013. Methods and concepts for the multi-criteria synthesis of ship structures. Ships Offshore Struct. 8 (3–4), 225–244.
Žanić, V., Grubišić, I., Trincas, G., 1997. Mathematical models for ship concept design. In: Proceedings of the 8th Congress of the International Maritime Association of Mediterranean, IMAM 97, Istambul, Turkey, pp. 7–16.
Žanić, V., Čudina, P., 2009. Multiattribute decision making methodology in the concept design of tankers and bulk carriers. Brodogradnja 60(1), 19–43.
Zaraphonitis, G., Marzi, J., Papanikolaou, A., Harries, S., Brunswig, J., 2020. Holistic ship design for life cycle. In: SNAME 6th International Symposium on Ship Operations, Management and Economics, SOME 2018, Athens, Greece.